The European Society of Cardiology Textbook of Cardiovascular Imaging

José Luis Zamorano
Jeroen J. Bax
Frank E. Rademakers
Juhani Knuuti (Eds.)

The ESC Textbook of Cardiovascular Imaging

Springer

Prof. José Luis Zamorano
Hospital Clinico San Carlos
Instituto Cardiovascular
C/Professor Martin Lagos, s/n
28040 Madrid
jlzamorano@vodafone.es
Jzamorano.hcsc@salud.madrid.org

Prof. Jeroen J. Bax
Leiden University
Medical Center
Dept. Cardiology
Albinusdreef 2
2333 ZA Leiden
Netherlands
j.j.bax@lumc.nl

Prof. Dr. Frank E. Rademakers
University Hospitals Leuven
Dept. Cardiology
Herestraat 49
3000 Leuven
Belgium
frank.rademakers@uzleuven.b

Prof. Dr. Juhani Knuuti
Turku University Hospital
Turku PET Centre
FI-20521 Turku
Finland
juhani.knuuti@tyks.fi

ISBN: 978-1-84882-420-1 e-ISBN: 978-1-84882-421-8
DOI: 10.1007/978-1-84882-421-8
Springer Dordrecht Heidelberg London New York

Library of Congress Control Number: 2009934506

Preface

Imaging is at the core of diagnostic procedures in cardiology. The idea of creating *The European Society of Cardiology Textbook of Cardiovascular Imaging* has, therefore, been in the air for quite a long time. We recognized the rapid development of cardiovascular imaging and the growth of the clinical use of cardiac imaging. Although there have been excellent books and reviews on the matter, the society experienced the need of a book representing the accumulated expertise of European cardiovascular imagers.

Our goal was to produce a clinically orientated book, which explained the utility of different imaging modalities in the diagnosis of all relevant major cardiovascular disorders. We invited the best specialists in the field to contribute with their expertise as authors.

The book is divided in sections that deal with specific themes involving theory and practice of cardiac imaging and its clinical use in all major cardiovascular diseases from coronary heart disease to cardiomyopathies.

We hope this book will become an ideal companion to all cardiologists, trainees, and cardiovascular imagers. There has been a lot of effort and hard work to develop this project. We are confident that this book will help to spread the expertise and knowledge available on cardiovascular imaging.

We thank all the authors who contributed long hours to develop the content of this book. Without their expertise and commitment, this book could not have been possible.

Madrid, Spain — José Luis Zamorano
Leiden, The Netherlands — Jeroen J. Bax
Leuven, Belgium — Frank E. Rademakers
Turku, Finland — Juhani Knuuti

Foreword

Images are a central part of our lives. Of the five senses, the eyes and vision have indeed triumphed over the others. We live, think, and dream through images.

Television captures our imagination and sends messages to us through images to the extent that there are now news reports in total silence. Television sound is often just a background noise. Newspapers, even the daily ones, communicate to us through catchy and colourful images. Often leaders and politicians care more about their image than their mission.

It is, therefore, not surprising that image has also invaded medicine and cardiology in particular. When I was a student, I thought that to be a good cardiologist one should have very good hearing to capture all of the abnormal heart sounds. This is no longer the case. The image of the echocardiogram has surpassed the stethoscope; the eyes have surpassed the ears. Today, technology is providing heart doctors with more and more sophisticated and fascinating images. So, to be a good cardiologist, you have to read this book!

I mean it. As it always happens in life, interaction is important. This is also true for cardiovascular images that need to be integrated within themselves and particularly with the patients. Without such interaction and integration even the most sophisticated image will be dull.

Interaction is what this book is about. Several European leaders explain to the reader, in a simple and comprehensive manner, the value and the benefit of different imaging modalities in the diagnosis of the most relevant cardiovascular diseases.

This book does something more as well. It describes a new subspecialty that we will all soon need: the imaging doctor, who will be able to interact with clinicians and help them resolve diagnostic dilemmas by choosing the right technique and by interpreting images in a patient-based manner.

As the president of the ESC, I thank the ECHO Association, the working groups, and the councils who are responsible for *The European Society of Cardiology Textbook of Cardiovascular Imaging.*

As a cardiologist, I thank all the authors and editors for contributing to develop the education of all cardiologists (myself included) through this book.

President Roberto Ferrari
European Society of Cardiology

Contents

Contributors

Stephan Achenbach, MD Medizinsche Klinik I, University of Erlangen, Erlangen, Germany

Luigi P. Badano, MD Echocadiography Laboratory, Cardiopulmonary Sciences, Azienda Ospedaliero-Universitaria, Udine, Italy

Helmut Baumgartner, MD Adult Congenital and Valvular Heart Disease Center, University of Muenster, Muenster, Germany

Prof. Jeroen J. Bax, MD, PhD Department of Cardiology, Leiden University Medical Center, Leiden, The Netherlands

Harald Becher, MD, PhD Department of Cardiovascular Medicine, John Ratcliffe Hospital, Oxford, UK

Frank M. Bengel, MD Division of Cardiovascular Nuclear Medicine, Johns Hopkins University Medical Institutions, Baltimore, MD, USA

Ruxandra T. Beyer, MD, PhD Cardiology-Intensive Care Unit, Heart Institute "N. Stancioiu", Cluy-Napoca, Romania

Amit Bhan, MD Department of Cardiology, King's College Hospital, London, UK

Jan Bogaert, MD, PhD Department of Radiology, Gasthuisberg University Hospital, Leuven, Belgium

Thomas Buck, MD Department of Cardiology, Division of Internal Medicine, West German Heart Center, University Clinic Essen, Essen, Germany

Peter Buser, MD Cardiology Department, University Hospital, Basel, Switzerland

Filippo Cademartiri, MD, PhD Radiology, Azienda Ospedaliero–Universitaria, Parma, Italy

Paolo Camici, MD Mrc Clinical Sciences Center, Imperial College School of Medicine Hammersmith Hospital, London, UK

Jean-Paul Carpenter, MD Royal Brompton Hospital, London, UK

Ignasi Carrio, MD Nuclear Medicine Unit, Hospital de Sant Pau, Barcelona, Spain

Pio Caso, MD Division of Cardiology, Monaldi Hospital, Naples, Italy

Paolo Colonna, MD Institute of Cardiology, Policlinico of Bari, Bari, Italy

Pim J. De Feyter, MD Radiology and Cardiology, Erasmus Medical Center, Rotterdam, The Netherlands

Genevieve Anne Derumeaux, MD Laboratre d'Echochardiographie, Hospital Louis Pradel, Lyon, France

Nuno Cortez Dias, MD Department of Cardiology, University Hospital Santa Maria, Lisbon, Portugal

Raimund Erbel, MD Department of Cardiology, West German Heart Center Essen, University Duiburg-Essen, Essen, Germany

Arturo Evangelista, MD Servei de Cardiologio, Hospital Vall d'Hebron, Barcelona, Spain

Frank Flachskampf, MD Universitaetsklinik Erlanger, Erlanger, Germany

Albert Flotats, MD Nuclear Medicine Department, Hospital Sant Pau, Barcelona, Spain

Miguel Garcia Fernandez, MD, PhD Department of Medicine, Universidad Compluterse de Madrid, Martinez Izquierdo 7 Bajo Deredro, Madrid, Spain

Covadonga Fernandez-Golfin, MD Cardiac Imaging Unit, Cardiovascular Institute Hospital Clinico San Carlos, Madrid, Spain

Mark Friedberg, MD Division of Cardiology, Hospital for Sick Children, Toronto, ON, Canada

Jerome Garot, MD Hospital Univesitaire Henri Mondor, Creteil, France

Michael A. Gatzoulis, MD, PhD Adult Congenital Heart Clinic, Royal Brompton Hospital, London, UK

Bernhard M. Gerber, MD Servize de Cardiologie, Cliniquis Univesitaires St. Luc, Woluwe St. Lambert, Belgium

Gilbert Habib, MD Service de Cardiologie B, C.H.U. de la Timone, Marseille, France

Rainer Hoffman, MD Aachen University, Prauwelsstrasse 30, Aachen, Germany

Majo Joseph, MD Department of Cardiovascular Medicine, Flinders Medical Center, Adelaide, Australia

Philipp Kaufmann, MD Cardiovascular Center, Nuclear Cardiology NUK C32, University Hospital Zurich, Zurich, Switzerland

Philip Kilner, MD Cardiovascular Magnetic Resonance Unit, Royal Brompton Resonance Unit, Royal Brampton Hospital, London, UK

Prof. Dr. Juhani Knuuti, MD, PhD Turku PET Centre, Turku University Hospital, Turku, Finland

Frederic Lamare, MD, PhD Division of Cardiovascular Nuclear Medicine, Johns Hopkins University Medical Institutions, Baltimore, MD, USA

Patrizio Lancellotti, MD, PhD Cardiology, University of Liege, Liege, Belgium

Paul Leeson, PhD, MRCP Department of Cardiovascular Medicine, John Radcliffe Hospital, Oxford, UK

Massimo Lombardi, MD MRI Laboratory, Clinical Physiology Institute, CNR National Research Council, Pisa, Italy

Erica Maffei, MD Department of Radiology, Erasmus Medical Center, Rotterdam, The Netherlands

Heiko Mahrholdt, MD Cardiology, Robert Bosch Medical Center, Stuttgart, Germany

David C. Maintz, MD Department of Clinical Radiology, University of Munster, Munster, Germany

Pedro Marcos-Alberca, MD, PhD Unidad de Imagen Cardiaca, Instituto Cardiovascular, Hospital Clinico San Carlos, Madrid, Spain

Chiara Martini, RT Radiology, Non-Invasive Cardio Imaging, Azienda Ospedaliera Di Parma, Parma, Italy

Thomas H. Marwick, MD Department of Medicine, Princess Alexandra Hospital, Brisbane, Australia

Julia Mascherbaur, MD Cardiology, Medical University of Vienna, Vienna, Austria

Luc Mertens, MD, PhD Cardiology, Hospital for Sick Children, Toronto, ON, Canada

Nico R. Mollet, MD, PhD Department of Radiology, Erasmus Medical Center, Rotterdam, The Netherlands

Mark Monaghan, MD Cardiology Care Group, Kings College Hospital, London, UK

Maric Moonen, MD Cardiology, University of Liege, Liege, Belgium

Denisa Muraru, MD Cardiology, Professor Dr. C.C. Iliescu Institute of Cardiovascular Diseases, Bucharest, Romania

Eike Nagel, MD Imaging Sciences, Rayene Institute, London, UK

Danilo Neglia, MD, PhD Cardiovascular PET Program, CNR, Pisa, Italy

Stefan Neubauer, MD Department of Cardiovascular Medicine, John Radcliffe Hospital, Oxford, UK

Ed Nicol, MD Cardiovascular Magnetic Resonance Unit, Royal Brompton Hospital, Sydney Street, London, UK

Petros Nihoyannopoulos, MD Imperial College School of Medicine, Hammersmith Hospital, London, UK

Alessandro Palumbo, MD, PhD Department of Radiology, Erasmus Medical Center, Rotterdam, The Netherlands

Dudley Pennell, MD Cardiovascular MR Unit, Royal Brompton Hospital, Sydney Street, London, UK

Leopoldo Perez de Isla, MD, PhD Unidad de Imagen Cardiovascular, Instituto Cardiovascular, Hospital Clinico San Carlos, Madrid, Spain

Pasquale Perrone-Filardi, MD Cattedra di Cardiologia, Universita Federico II, Naples, Italy

Luc Pierard, MD, PhD Cardiology, University of Liege,
Liege, Belgium

Fausto Jose Pinto, MD Department of Cardiology, Lisbon Cardiovascular Institute, Lisbon, Portugal

Don Poldermans, MD Department of Anesthesiology, Erasmus Medical Center, Rotterdam, The Netherlands

Björn Plicht, MD Cardiology Clinic, West German Heart Center, University Clinic Essen, Essen, Germany

Sanjay Prasad, MD CMR Unit, Royal Brompton Hospital, Sydney Street, London, UK

Prof. Dr. Frank E. Rademakers, MD, PhD Department of Cardiology, University Hospitals Leuven, Herestraat 49, 3000 Leuven, Belgium

Raphael Rosenhek, MD Department of Cardiology, Medical University of Vienna, Vienna, Austria

Michael Rubens, MD Cardiovascular Magnetic Resonance Unit, Royal Brompton Hospital, Sydney Street, London, UK

Juerg Schwitter, MD Department of Internal Medicine, University Hospital Zurich, Zurich, Switzerland

Roxy Senior, MD Department of Cardiology, Northwick Park Hospital, Harrow Middlesex, UK

Rosa Sicari, MD Echocardiography, CUR, Institute of Clinical Physiology, Pisa, Italy

Udo Sechtem, MD Abteilung Fuer Kardiologie Und Pulmologie, Robert Bosch Krankenhaus, Stuttgart, Germany

Joseph Selvanayagam, MD Department of Cardiovascular Medicine, Flinders Medical Center, Adelaide, Australia

Marta Sitges, MD Cardiology Department, Hospital Clinic-University of Barcelona, Barcelona, Spain

James Elliot Stirrup, MRCP, MB, BS, BSC Nuclear Medicine, Royal Brompton Hospital, Sydney Street, London, UK

Edgar Tay, MD Adult Congenital Heart Disease, Royal Brompton Hospital, London, UK

Frank Thuny, MD Service de Cardiologie B, Département de Cardiologie, C.H.U. de la Timone, Marseille, France

Stephen Richard Underwood, MA, MD Department of Nuclear Medicine, Royal Brompton Hospital, London, UK

Nico Van de Veire, MD, PhD Department of Cardiology, Leiden University Medical Center, Leiden, The Netherlands

Ernst E. van der Wall, MD, PhD Department of Cardiology, Leiden University Medical Center, Leiden, The Netherlands

Albert C. Van Rossum, MD Department of Cardiology, VU Medical Center, Amsterdam, The Netherlands

Jeremy J. Wright, MB, BS(Hons) Hearts 1st, Greenslopes Private Hospital, Greenslopes Brisbane, Australia

Ali Yilmaz, MD Abteiling fuer Kardiologie und Pulmologie, Robert Bosch Krankenhaus, Stuttgart, Germany

Prof. José Luis Zamorano, MD, PhD Cardiovascular Institute, Hospital Clinico San Carlos, Madrid, Spain

Section 1

Technical Aspects of Imaging

Chapter 1

ECHOCARDIOGRAPHY: BASIC PRINCIPLES

Miguel Angel García-Fernández and Pio Caso

CONTENTS

J. L. Zamorano et al. (eds.), *The ESC Textbook of Cardiovascular Imaging*
DOI: 10.1007/978-1-84882-421-8_1, © Springer-Verlag London Limited 2010

Introduction

Echocardiography is a useful technique for the examination of the heart of patients of all ages. Good-quality images are required and transducer positions must be adapted to each patient.

A variety of transducers are available with different widths, ultrasound emission frequencies, and focal characteristics. Transducer width is based on ultrasound emission frequency, and it is important to consider the relationship between resolution and penetration in order to choose frequencies appropriate for a given examination. Resolution is the ability to distinguish between adjacent structures, while ultrasound penetration measures the ability of the ultrasound beam to pass through different cardiac structures. An increase in ultrasound emission frequency leads to an increase in image resolution. If attenuation also increases, however, there is a reduction in ultrasound penetration.

Echocardiographic examination usually requires a frequency of at least 2.0 MHz, but it can change depending on the patient's chest characteristics. In a child or thin adult, a 3–5 MHz transducer can be used with good resolution and penetration. A 7–7.5 MHz transducer produces better-quality images in a newborn, while a 2–2.5 MHz transducer is optimal for an obese adult.

Second harmonic imaging is an echocardiographic tool used to improve technically difficult images. For example, a transducer with second harmonic echocardiography transmits ultrasound at 1.8 MHz (plus penetration) and receives a 3.6 MHz signal with improvement in image quality. Moreover, it is essential to set ultrasound emission frequency low when using Doppler technique, as lower frequencies are required to register high-velocity flows. Following the selection of an appropriate transducer, gray scale gains and depths are manually controlled to an adequate delineation of structures to be visualized.

Echocardiographic examination is usually performed with the patient in left lateral decubitus position and with 30° flexion of the chest in order to situate the heart nearer to the anterior chest wall. The patient's left arm is placed under the head so as to widen intercostal spaces. A different transducer position may be used during a conventional echocardiographic exam (Fig. 1.1).[1,2] The examination begins by placing the transducer on the third or fourth intercostal space of the left parasternal line (left parasternal window) and subsequently on the apex (apical window). Such images are obtained with the patient in left lateral position (Fig. 1.2).

Sub-costal and supra-sternal windows may be obtained with the patient in supine position. A sub-costal approach is useful for visualizing inferior vena cava, hepatic veins, and congenital abnormalities, as well as in patients with low diaphragm or bad acoustic window due to respiratory

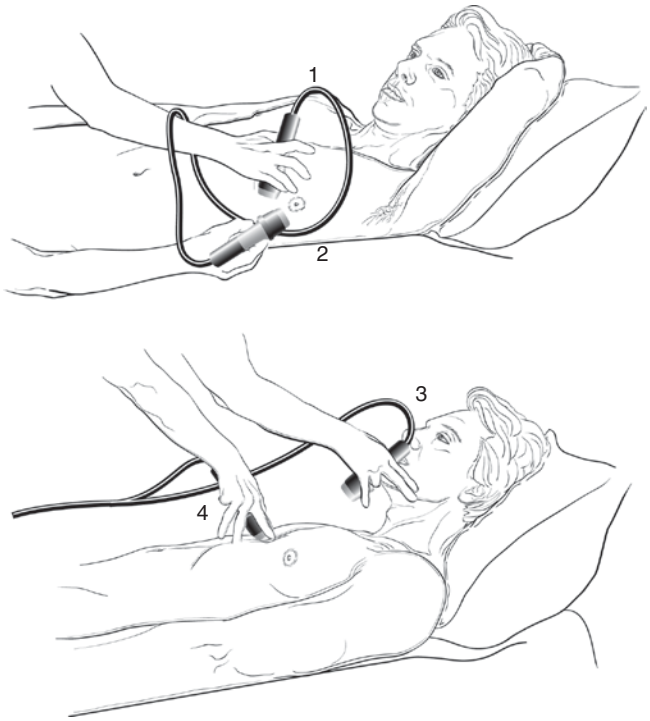

Fig. 1.1 Transthoracic transducer standard positions for obtaining different planes. Parasternal (*position 1*) and apical planes (*position 2*) are obtained with the patients in left lateral position. Supra-sternal (*position 3*) and subxiphoid planes are usually obtained with the patient in supine position (*position 4*)

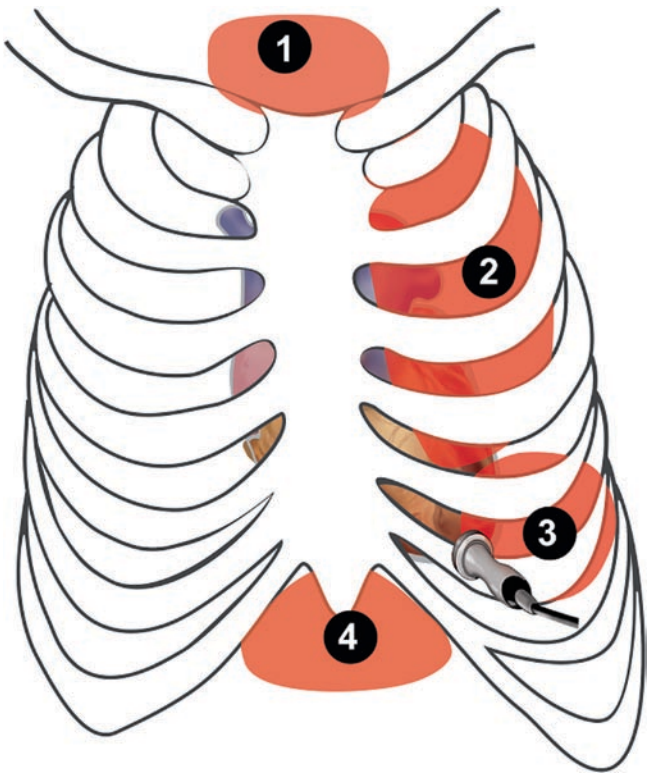

Fig. 1.2 Anatomic structures and transthoracic transducer positions for obtaining parasternal views (*position 2*), apical views (*position 3*), supra-sternal views (*position 1*), and subxiphoid views (*position 4*)

diseases.[3,4] The supra-sternal approach places the patient's head in retroflexion and permits an observation of the base of the heart and great vessels.[5] Finally, the right parasternal window is useful for visualizing the aorta and inter-atrial septum and is obtained by placing the patient in right lateral position.[6,7]

M-Mode Echocardiography

M-mode echocardiography was described at the end of the 1950s[8] and introduced into clinical practice at the beginning of the 1960s. M-mode was the only technique used during echocardiographic study for 20 years, but current echocardiographic study includes different techniques such as 2D, Doppler, and colour-flow Doppler imaging. M-mode, however, remains a very useful part of ultrasound examination. M-mode echocardiography is able to evaluate rapid motion of cardiac structures because sampling rate is higher than in 2D echo, and it can show movement in thin structures such as the cardiac valves. The method is based on transmission of echo in a single line. Returning echoes are displayed on a graph in which structural depth and movement in time are reliably represented.

The routine cardiac examination with M-mode shows images of four cardiac chambers and cardiac valves. A better evaluation is obtained with the probe guided by 2D echo image in parasternal view, perpendicular to cardiac structure. It is sometimes necessary to move the probe tip from a different intercostal space in order to determine the best position with perpendicular incident echoes through cardiac structures.

Aortic Valve

Aortic valve, left atrium, and aortic root are well evaluated when the cursor is perpendicular to the aortic root. An M-mode recording through the aortic root at the level of valve leaflets shows aortic walls in parallel moving anteriorly in systole and posteriorly in diastole. Aortic valve leaflet coaptation in M-mode is seen as a thin single line in diastole and a double line in systole that separate rapidly and completely, forming a box-like appearance (Fig. 1.3). It is possible to evaluate the pre-ejection time (from EKG q wave to beginning of aortic valve opening) and ejection time (period in which the aortic leaflets are opened). The left atrium is posterior to the aortic root and shows filling during atrial diastole (ventricular systole) and emptying in atrial systole (ventricular diastole). Anterior displacement of the aortic root is due to left atrial filling. This anterior movement is increased when there is increased filling (mitral regurgitation) or decreased in case of decreased cardiac output.

Mitral Valve

The mitral valve can be studied in parasternal view by placing the cursor perpendicular to the septum and mitral leaflets. The ultrasonic beam transverses the anterior thorax, right ventricle, inter-ventricular septum, anterior mitral leaflet, posterior mitral leaflet, posterior wall of left ventricle, and the pericardium (Fig. 1.4).

The leaflets of mitral valve separate widely with maximum early-diastolic motion of the anterior leaflet, termed E point. The leaflets move together in the centre of the left ventricle and then separate again after atrial systole (A wave).

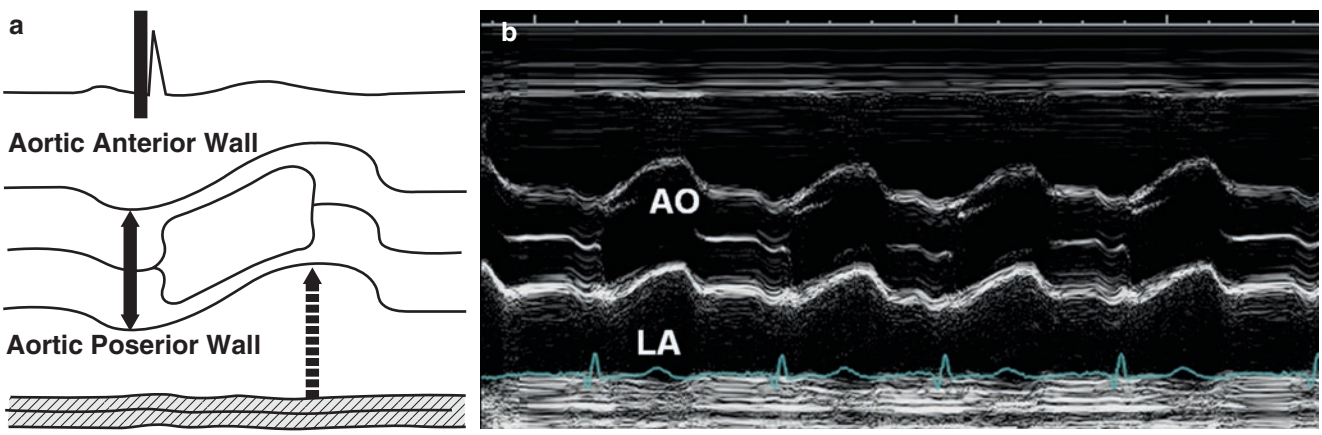

Fig. 1.3 **(a)** Diagram of aortic valve and left atrium. Cursor transects anterior aortic wall, aortic valve, posterior aortic wall, left atrium, and posterior wall of left atrium. **(b)** Aortic valve plane in M-mode. It is possible to show aortic leaflets as a box in systole and thin line in diastole. *AO* aorta; *LA* left atrium

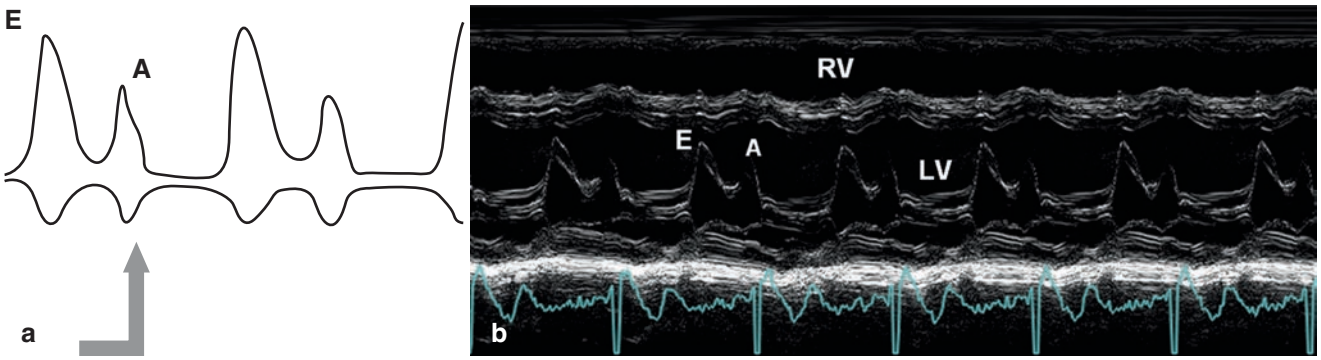

Fig. 1.4 **(a)** Diagram of mitral valve. **(b)** Mitral valve in M-mode, opening in diastole in the centre of left ventricle. The leaflets of mitral valve separate widely with maximum early-diastolic motion of anterior leaflet called E point. The leaflets move together in the centre of left ventricle and then separate again after atrial systole (A wave). *RV* right ventricle; *E* early mitral diastolic wave; *A* late diastolic mitral valve wave; *LV* left ventricle

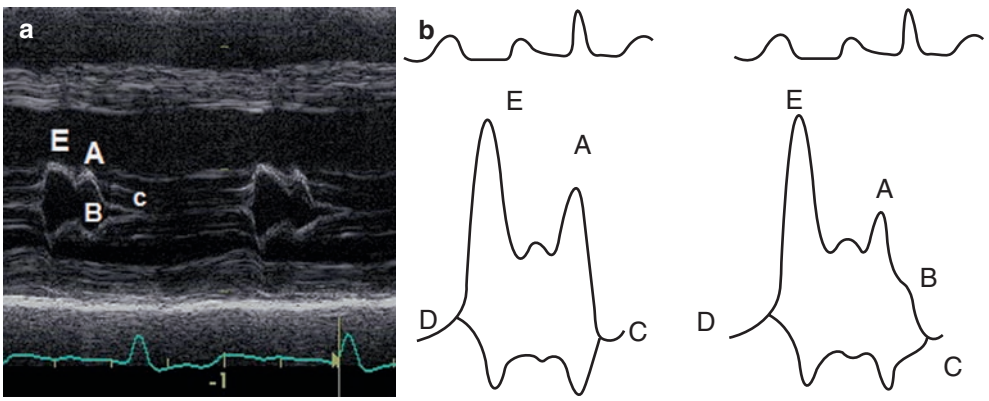

Fig. 1.5 Diagram of mitral valve opening in normal patient and in patients with ventricular dysfunction. In normal patients, the leaflets of mitral valve separate widely with maximum early-diastolic motion of anterior leaflet (E point). Distance between E point and septum is usually short. Leaflets move together in the centre of left ventricle and then separate again after atrial systole (A wave). The slope from A point to mitral closure (C point) is linear. In patients with left ventricular dysfunction and high left ventricular end-diastolic pressure, the slope from A to C presents a B bump or shoulder. M-mode (b) of a patient with left ventricular dysfunction and high end-diastolic pressure with characteristic shoulder on A-C line (B point). The distance between E wave and septum is greater. *D* opening point of mitral valve; *E* point is the maximum early-diastolic motion of anterior leaflet; *A* point is the late diastolic motion of anterior leaflet of mitral valve; *C* point is the closure of mitral valve; *B* point is the shoulder of A-C slope

The slope from A point to mitral closure (C point) is linear unless left ventricular end-diastolic pressure is elevated. In this case, a B bump or an A-C shoulder can be seen (Fig. 1.5). In systole, the leaflets of the mitral valve are seen as a thin line that moves slightly forward during systole.

Left Ventricle

Measurements of the left ventricular cavity dimensions, thickness of septum and posterior wall, volumes, and mass can be readily derived from M-mode recordings. These measurements are limited because they represent a single line evaluation through the septum and, in case of abnormal regional contraction, can be misleading.

For better reproducibility of M-mode evaluation, morphologic and temporal criteria have been established: (1) cursor perpendicular to septum and left ventricle, (2) diastolic measures at the beginning of QRS, and (3) systolic measures at highest excursion of posterior wall endocardium. The ventricular border of septum (as anterior line) and the ventricular border of posterior wall (as posterior line) can be used to evaluate left ventricular diameters. It is important to distinguish between mitral chordae and anterior border of the posterior wall (Fig. 1.6). The cavity dimensions can be used to calculate ejection fraction, but this measure involves assumptions that do not always hold (Tables 1.1–1.4). With the transducer placed along the left sternal border and in the third or fourth intercostal space, we can sweep the ultrasonic beam in a sector between the base of the heart and the apex (Fig. 1.7).

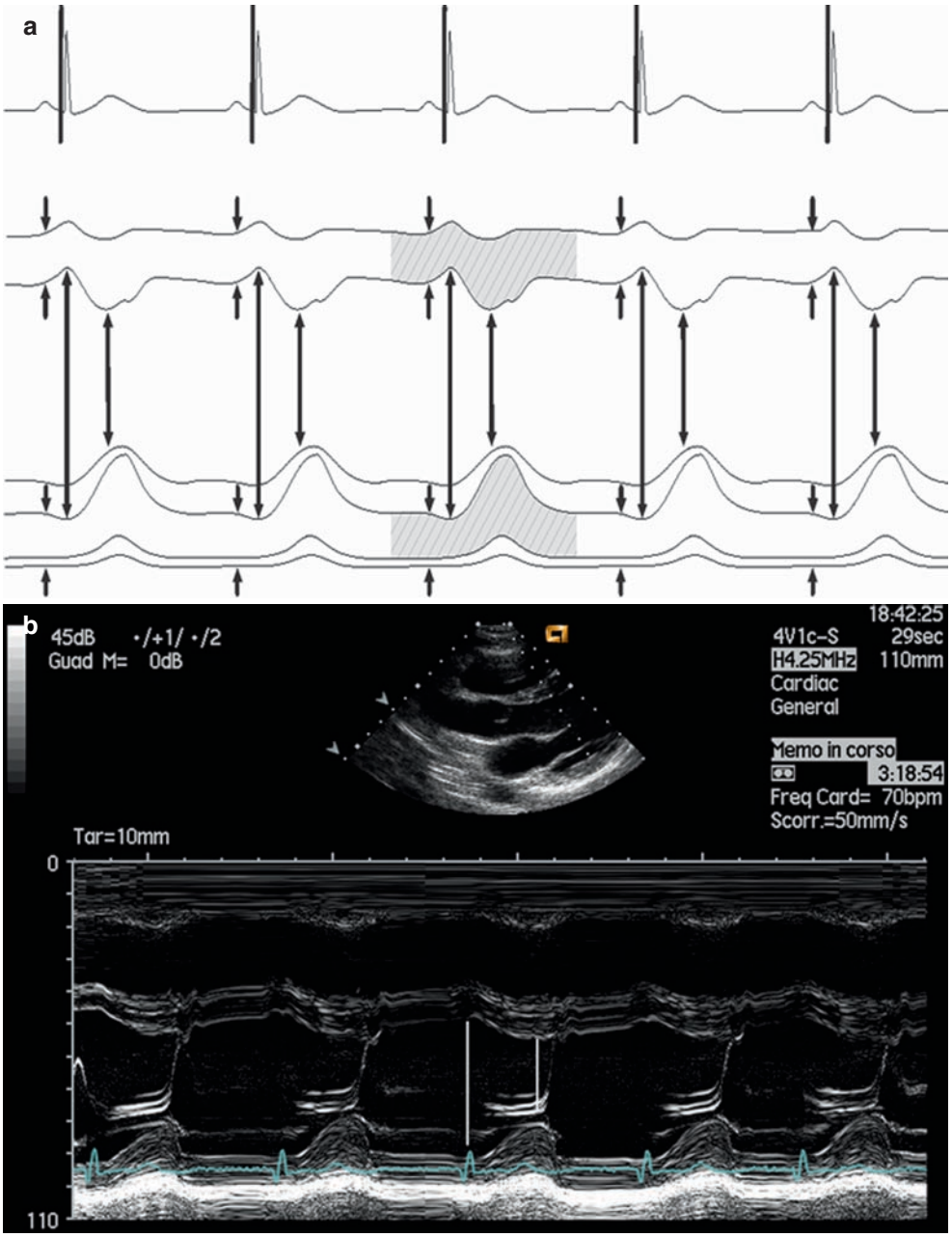

Fig. 1.6 **(a)** Diagram of left ventricle. The *arrows* show measures of end-systolic and end-diastolic diameters of left ventricle and thickness of septum and posterior wall. For evaluation of left ventricular diameters, the ventricular border of septum and ventricular border of posterior wall are used as *anterior line* and *posterior lines*, respectively. **(b)** Left ventricle measures in M-mode. Diastolic measures are taken at the beginning of QRS and systolic measures are taken where higher excursion of posterior wall endocardium can be seen. The *long and short lines* show left ventricle end-diastolic diameter and left ventricle end-systolic diameter, respectively

Table 1.1. Normal M-mode values[9,10]

	≤30 years	>70 years	M	F
			N = 288	*N* = 524
LVID (mm)	48 ± 5.6	45.3 ± 5.6	50.8 ± 3.6	46.1 ± 3
LVSS (mm)	30 ± 5.8	28.4 ± 5.8	32.9 ± 3.4	28.9 ± 2.8
IVS thickness (mm)	9.8 ± 1.7	11.8 ± 1.7	9.5 ± 3.5	8.5 ± 3
PW s (mm)	10.1 ± 1.4	11.8 ± 1.4	9.5 ± 2.5	8.5 ± 3.5
Aorta	27.4 ± 5.7	33.5 ± 5.7	32 ± 3	28 ± 3
Left atrium	34.3 ± 7	39.7 ± 7	37.5 ± 3.6	33.1 ± 3.2

LVID left ventricular internal dimension, end diastole; *LVSS* left ventricular internal dimension, end systole; *IVS* inter-ventricular septum; *PW* posterior wall; *M* male; *F* female

Table 1.2. Ventricular mass and myocardial dimension[33]

	n	g/m2	g/m	SIV (mm)	PP (mm)	LVID (mm)
Man						
Total	47	99 ± 15(129)	108 ± 17	10.2 ± 1.2	9.9 ± 1	51 ± 3
<50a	27	97 ± 14(124)	107 ± 15	10.1 ± 0.9	9.6 ± 0.8	52 ± 3
≥50a	20	102 ± 17(135)	111 ± 20	10.4 ± 1.5	10.2 ± 1.1	51 ± 3
Woman						
Total	64	88 ± 15(129)	89 ± 17	9.2 ± 1.2	8.9 ± 0.9	47 ± 4
<50a	34	82 ± 13(108)	83 ± 14	8.6 ± 0.7	8.6 ± 0.7	47 ± 3
≥50a	30	93 ± 16(124)	96 ± 18	9.8 ± 0.9	9.2 ± 0.9	47 ± 4

LVID left ventricular internal dimension, end diastole; *LVSS* left ventricular internal dimension, end systole; *IVS* inter-ventricular septum; *PW* posterior wall

Table 1.3. Left ventricular volumes[15]

	End-diastolic	End-systolic
Apical 4-chamber (cc)		
Man	112 ± 27	35 ± 16
Woman	89 ± 20	33 ± 12
Apical 2-chamber (cc)		
Man	130 ± 27	40 ± 14
Woman	92 ± 19	31 ± 11
Biplane (Simpson)		
Man	110 ± 22	34 ± 12
Woman	80 ± 12	29 ± 10

Right Ventricle

Diastolic diameter can be measured along the same lines as for left ventricular diastolic measures. The anterior border of right ventricle is not clearly visible in many cases and the position of right ventricle is sometimes oblique. The different alignment between the cursor and the right ventricle yields high measurement variability (Fig. 1.6).

Tricuspid Valve

The tricuspid valve can be recorded from the initial position and by angulating the transducer inferomedially. The tricuspid valve's M-mode image is similar to that of the mitral valve and uses the same nomenclature (Fig. 1.8).

Pulmonary Valve

The posterior leaflet of the pulmonary valve can be seen with the transducer in the initial position and by tilting slightly superiorly and laterally. The leaflet moves to a posterior position in systole and to an anterior position in diastole. *A wave* is the expression of atrial contraction and is signed after EKG *p wave. Point b* occurs at the beginning of systole. *Point c* marks maximal excursion. *Point d* occurs at the end of systole and posterior closure is labelled *Point e.* During diastole and just before atrial contraction, the leaflet moves posteriorly with maximum excursion and is denoted as *Point f.* As stated previously, slight displacement of the leaflet in diastole is referred to as *a wave.* This wave is increased when pulmonary stenosis is present, and decreased

Table 1.4. Left ventricular dimension and body surface (m^2)[11]

		1.4–1.6 m^2	1.61–1.8 m^2	1.81–2.0 m^2
Long axis (mm)	Diastole Systole	34–49 23–39	36–51 24–41	39–53 25–44
Short axis (mm)	Diastole Systole	35–55 23–39	38–58 24–40	41–61 26–41
Four chamber (mm)	Diastole Systole	59–83 45–69	63–87 46–74	66–90 46–79

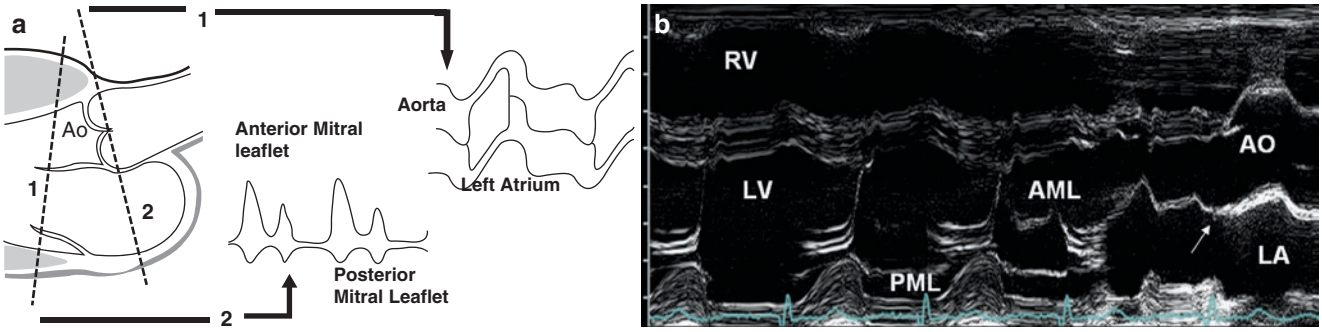

Fig. 1.7 Standard sweep from left ventricle and mitral valve to aorta and aortic valve. **(a)** Diagram of moving cursor line from left ventricle (*line 1*) to aorta (*line 2*). It is possible to measure all important diameters of the left and right ventricle, aorta, and left atrium. **(b)** M-mode of moving cursor line from left ventricle to mitral valve and aorta. The mitral valve appears in the centre of the left ventricle and aortic valve appears in the centre of the aorta. Line of continuity between AML and posterior aortic wall is evident. *Large arrow* in the diagram shows probe movement from mitral valve to aortic valve; thin arrow in M-mode shows continuity between anterior leaflet of mitral valve and posterior aortic wall. *AO* aortic valve; *LA* left atrium; *LV* left ventricle; *RV* right ventricle; *AML* anterior mitral valve leaflet; *PML* posterior mitral valve leaflet

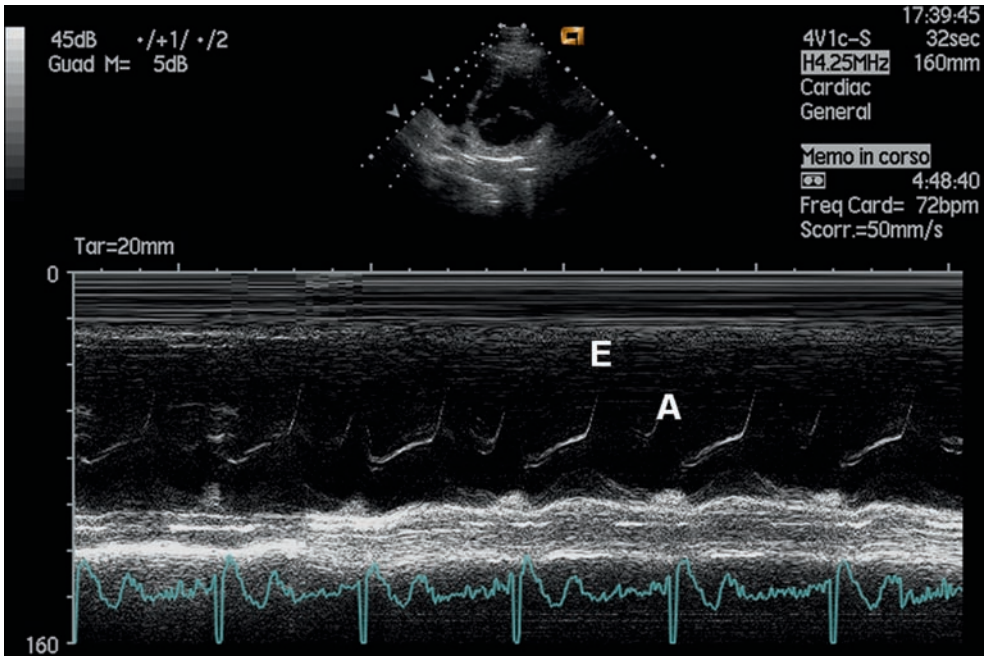

Fig. 1.8 Tricuspid valve M-mode image is similar to mitral valve image and uses the same nomenclature. E point is the maximum early-diastolic motion of tricuspid valve. A-point is the late diastolic motion of tricuspid valve

when pulmonary hypertension is present. In the latter case, midsystolic closure of the pulmonary valve is seen. Finally, it is possible to evaluate pre-ejection period from EKG *q wave* to *Point b,* and ejection period can be measured from *Point b* to *Point e* (Fig. 1.9).

Two-Dimensional Echocardiography

Two-dimensional echocardiography offers the possibility of real-time high resolution imaging of cardiac structure and function. It is the basis of the study of cardiac imaging with ultrasound, as it is the reference for analysis of cardiac flow with pulsed-wave Doppler (PWD), continuous-wave Doppler (CWD), and colour-flow Doppler.

Preference of image orientation in 2D echocardiography varies from one echo laboratory to another one. Recommendations for echocardiographic image orientation which were established by the American Society of Echocardiography[12] will be herein adhered to in the description of different echocardiograhic imaging planes. There are three basic imaging slices utilized for obtaining such images[13,14]: long axis (from the aorta to the apex), short axis, and 4-chamber (Fig. 1.10).

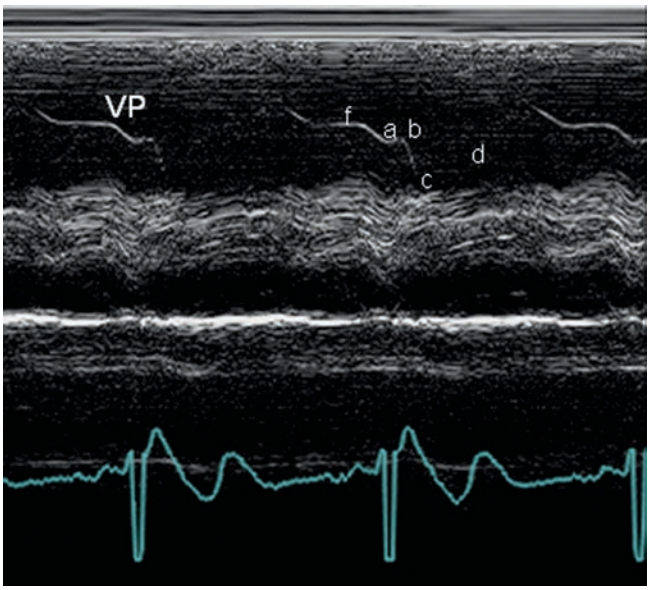

Fig. 1.9 The pulmonary valve is observed in short-axis parasternal view under the guide of 2D images. It is possible to follow the anterior and posterior excursions of the posterior leaflet in systole and diastole, respectively. *A wave* is atrial contraction (after EKG p wave); *b point* is at the beginning of systole; *point d* is the end of systole; *f point* is in diastole before atrial contraction and is maximum posterior displacement of the valve

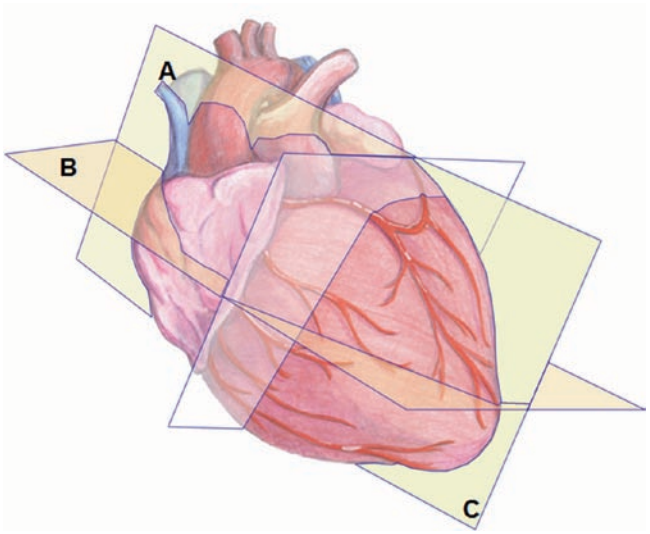

Fig. 1.10 Tomographic image planes used in a 2D echocardiographic study. *A* long axis; *B* short axis; *C* 4-chamber

Parasternal Long-Axis View

In this view (Fig. 1.11), the ultrasound scan plane intersects an imaginary line drawn from the right shoulder to the left hip and represents a long-axis section of the left ventricle. A large number of cardiac structures that do not lie precisely in the scan plane can be visualized at this level. Due to variations in patient anatomy, slight re-positioning of the transducer must be performed for image optimization.

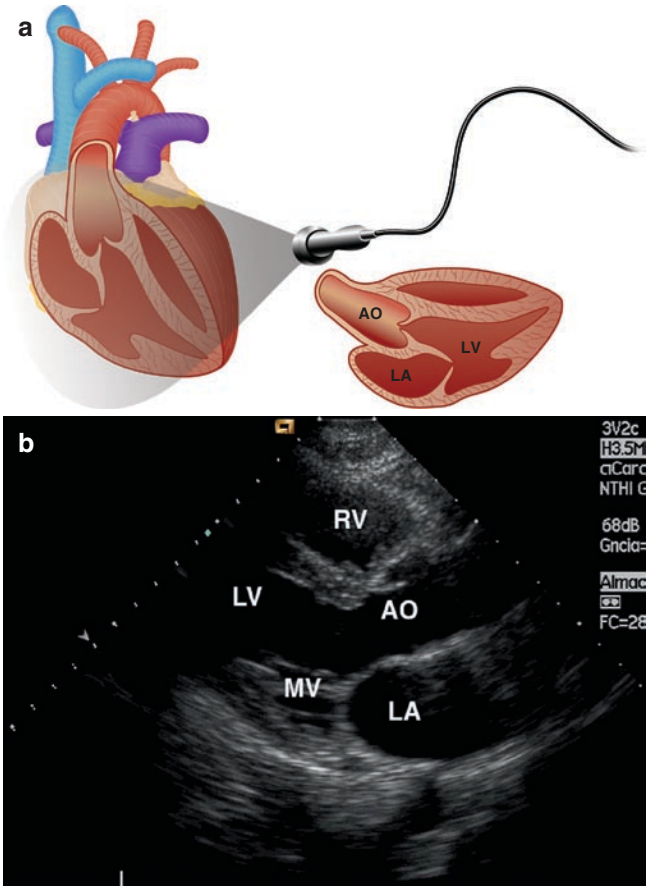

Fig. 1.11 **(a)** Schematic anatomic section of a parasternal long-axis view. **(b)** Corresponding still-frame of a 2D echocardiography of the parasternal long-axis view. *AO* aortic valve; *RV* right ventricle; *LA* left atrium; *MV* mitral valve; *LV* left ventricle

The *right ventricle* is located in the region closest to the transducer. The *left atrium* can be seen in the far right region of the image. In some cases, it is possible to visualize a round structure representing the left inferior pulmonary vein immediately posterior to left atrium. The *aortic valve* and *ascending thoracic aorta* can be viewed between left atrium and right ventricle. The aortic valve can be visualized during systole as two linear echocardiographic images parallel to the walls of the ascending thoracic aorta. The *right coronary cusp* and non-coronary cusp can be viewed in the regions closest to and farthest from the transducer, respectively. A linear echodense image can be observed at level of cusp closure during diastole. The *anterior* and *posterior leaflets* of the *mitral valve* can also be identified in this imaging plane, as well as the *tendinous chords* and their fusion with *papillary muscle.* The *left ventricular outflow tract* is situated between the inter-ventricular septum and anterior mitral leaflet, which are observed in the anterior and posterior positions of the image, respectively. The left ventricle is found in the left area of the image when the inter-ventricular septum and posterolateral wall are placed proximal and distal to the transducer, respectively. The *pericardium* appears at the lower edge of the image

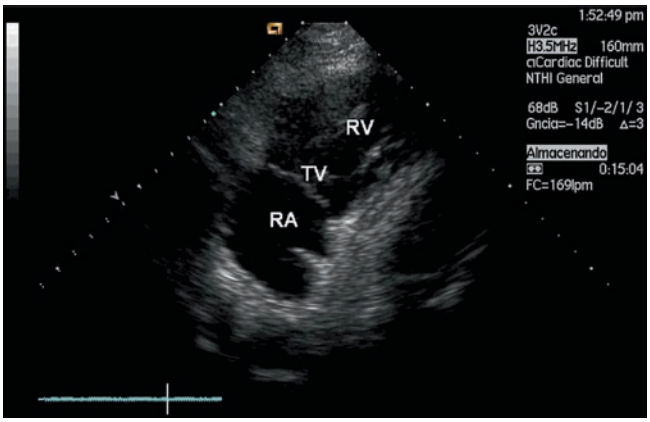

Fig. 1.12 Long-axis view of the right ventricle and right atrium. *RA* right atrium; *RV* right ventricle; *TV* tricuspid valve

where the descending thoracic aorta is also sometimes visible. The *coronary sinus* can be visualized as an echo-free structure at atrio-ventricular groove level and follows the motion of the atrio-ventricular ring.

Long-axis views of the *right ventricle* and *right atrium* are obtained upon slight inferomedial rotation of the transducer. In this view, the right atrium is observed in the right posterior region of the image, while the right ventricle apex appears in the extreme upper left-hand corner. It is also possible to detect the orifice of the inferior vena cava and Eustachian valve in the posterior wall of the right atrium. This image plane permits the assessment of *inferior* and *anterior right ventricle walls* and *inflow tract,* as well as of anterior and posterior leaflets of the tricuspid valve (Fig. 1.12).

Parasternal Short-Axis View

The parasternal short-axis view is obtained upon 90º clockwise rotation of the transducer from its initial position. The ultrasound scan plane now intersects an imaginary line drawn from the left shoulder to the right hip. Four different imaging planes are made possible by slightly tilting the transducer.

The base of the heart can be visualized by tilting the transducer towards the right shoulder within what is termed *parasternal short-axis plane at level of aorta* (Fig. 1.13). The aortic valve, located anterior to left atrium and posterior to right ventricle, is observed in the central region of the image along with its three leaflets (in a Y-shape configuration): right coronary at the lower left, coronary in the upper region, and non-coronary in the left region of the image. This imaging plane permits the measurement of aortic root size, detection of morphological alterations of Valsalva sinus (aneurysms, etc.), and diagnosis of proximal aortic dissection. Congenital anomalies of the aortic valve and valve leaflet abnormalities can also be assessed.

The *tricuspid valve* is observed to the left of the aortic valve. Coursing leftward and anterior to the aortic root is the right ventricular outflow tract. Rightward and anterior to the aortic valve, a portion of the *pulmonary valve* can be seen. The main *pulmonary artery* curves around the aorta and its two principal branches (*right* and *left pulmonary arteries,* respectively) can be observed. The left atrium is seen posterior to the aortic valve and separated from the right atrium by the atrial septum. In spite of the fact that the parasternal short-axis imaging plane was originally indicated for the assessment of septal defects (atrial septal defect, patent

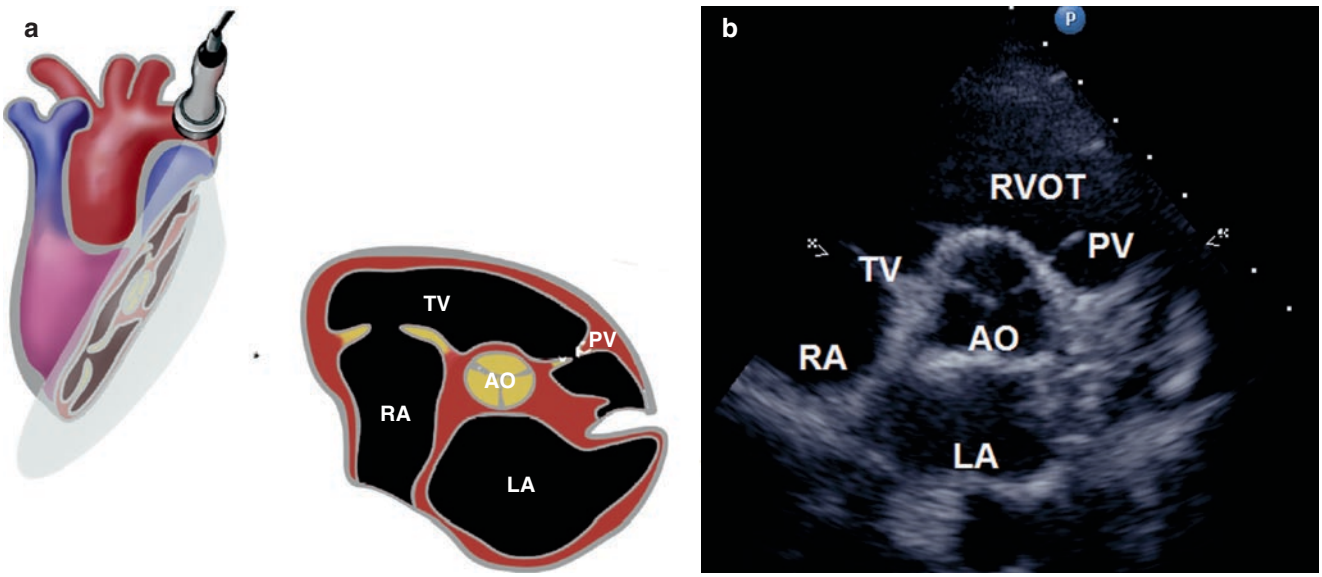

Fig. 1.13 **(a)** Schematic anatomic section of a parasternal short axis plane through the base of the heart. **(b)** Corresponding still-frame of a 2D echocardiography of parasternal short-axis plane at the base of the heart. *AO* aortic valve; *RA* right atrium; *RV* right ventricle; *LA* left atrium; *TV* tricuspid valve; *PV* pulmonary valve; *RVOT* right ventricular outflow tract

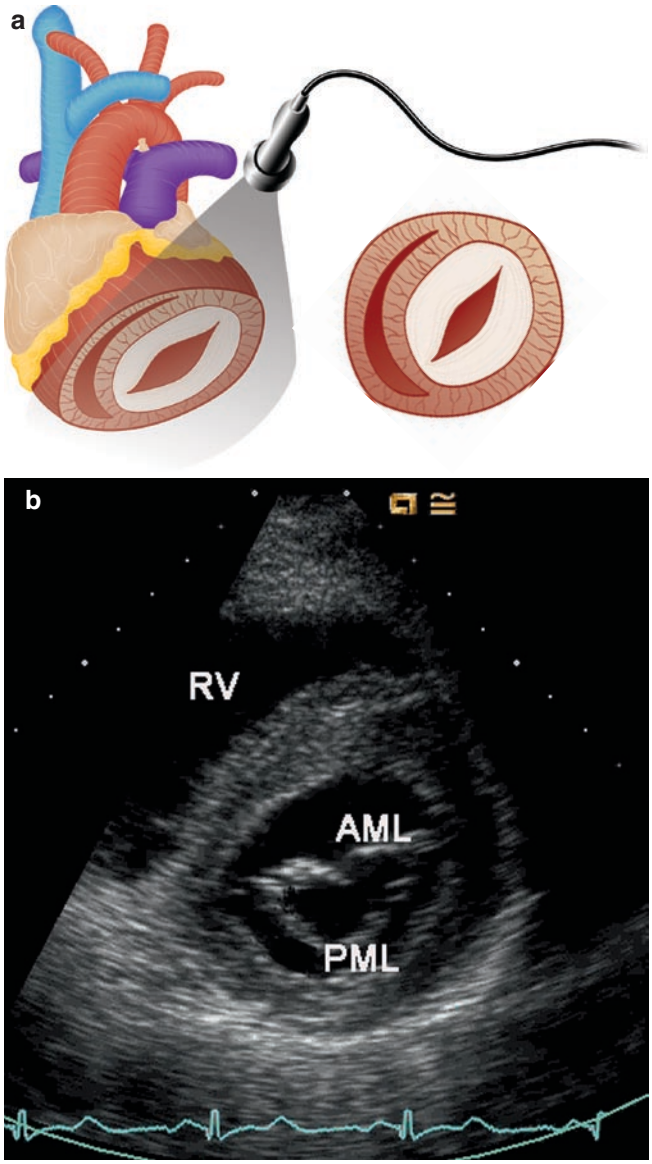

Fig. 1.14 **(a)** Schematic anatomic section of a parasternal short-axis plane through the mitral valve. **(b)** Corresponding still-frame of a 2D echocardiography of parasternal short-axis plane at the mitral valve level. *RV* right ventricle; *AMV* anterior mitral valve leaflets; *PMV* posterior mitral valve leaflets

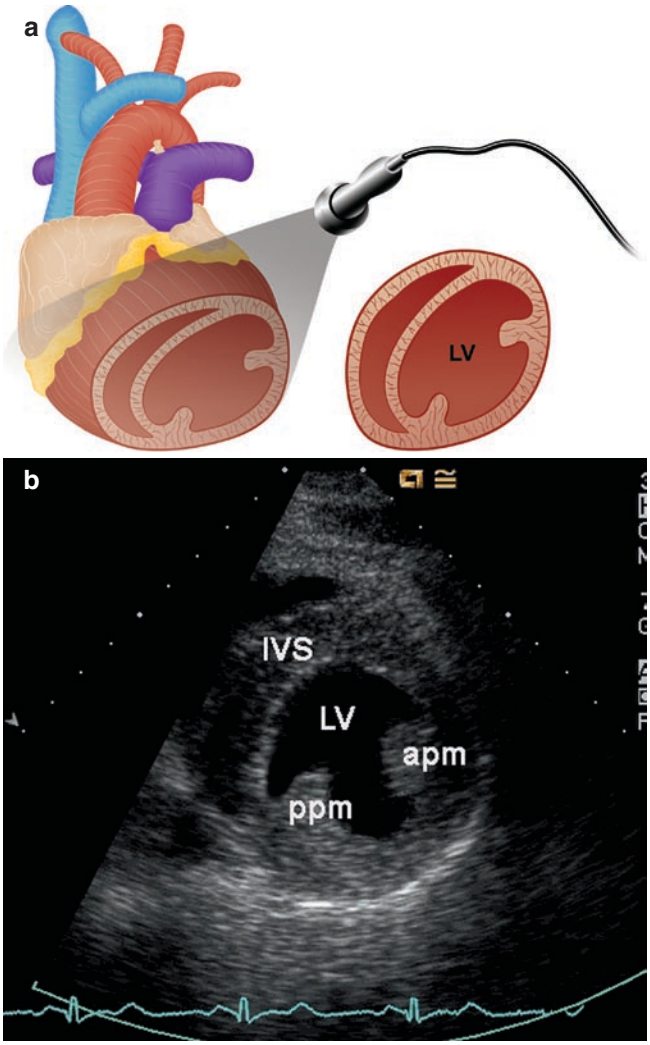

Fig. 1.15 **(a)** Schematic anatomic section of a paraesternal short-axis plane through papillary muscle level. **(b)** Corresponding still-frame of a 2D echocardiography of the parastenal short-axis plane at the papillary level. *IVS* inter-ventricular septum; *apm* anterior papillary muscle; *ppm* posterior papillary muscle

foramen ovale), these are analyzed more adequately with apical 4-chamber and sub-costal imaging.

An inferior and rightward tilting of transducer results in a *parasternal short-axis view at the level of the mitral valve* (Fig. 1.14). The mitral valve is observed with the septal leaflet in anterior position and posterior leaflet in the lower portion of the image (whose form has been commonly likened to a fish mouth). Tilting the transducer more parallel to the direction of blood flow, it is possible to identify the *left ventricle* as well as antero-lateral and postero-medial papillary muscles located inside the ventricular cavity at the 3 and 8 o′clock positions, respectively (Fig. 1.15). The right ventricle (anterior, lateral, and posterior segments) can be identified in the left anterior portion of the image and is separated from the left ventricle by the inter-ventricular septum. Figure 1.16 shows the different segments of the left ventricle, which can be observed in the short-axis view at mitral, papillary muscle, and apical levels.

Apical Views

The apical imaging plane is obtained with the patient in left lateral decubitus position. The ultrasound scan plane intersects an imaginary line that runs superiorly and medially from the left median axillary line to the right scapula of the patient. The transducer is placed tangentially in the fifth intercostal space along the median axillary line at apical level. It is useful in some patients to locate the cardiac apex and place the transducer nearest to the point of maximum apical impulse. Another way of locating the apex (in cases where palpitation is inadequate) consists of progressively sliding the transducer from parasternal short-axis plane position.

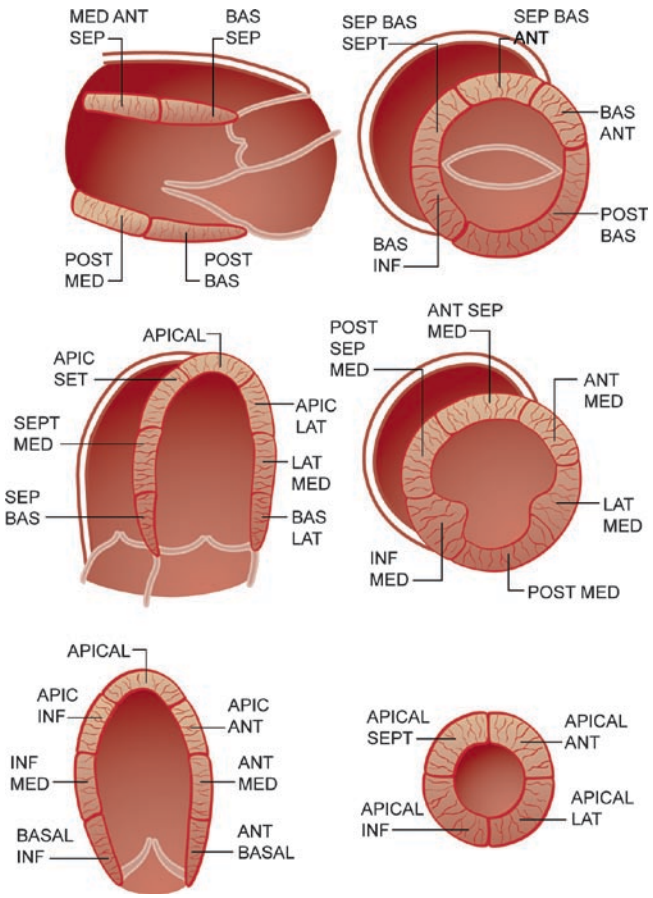

Fig. 1.16 Schematic diagram of the 16 segment model for regional wall motion analysis. The myocardium is divided into different levels: basal, mid-, or papillary muscle, and apical. The different segments can be analyzed from multiple tomographic planes

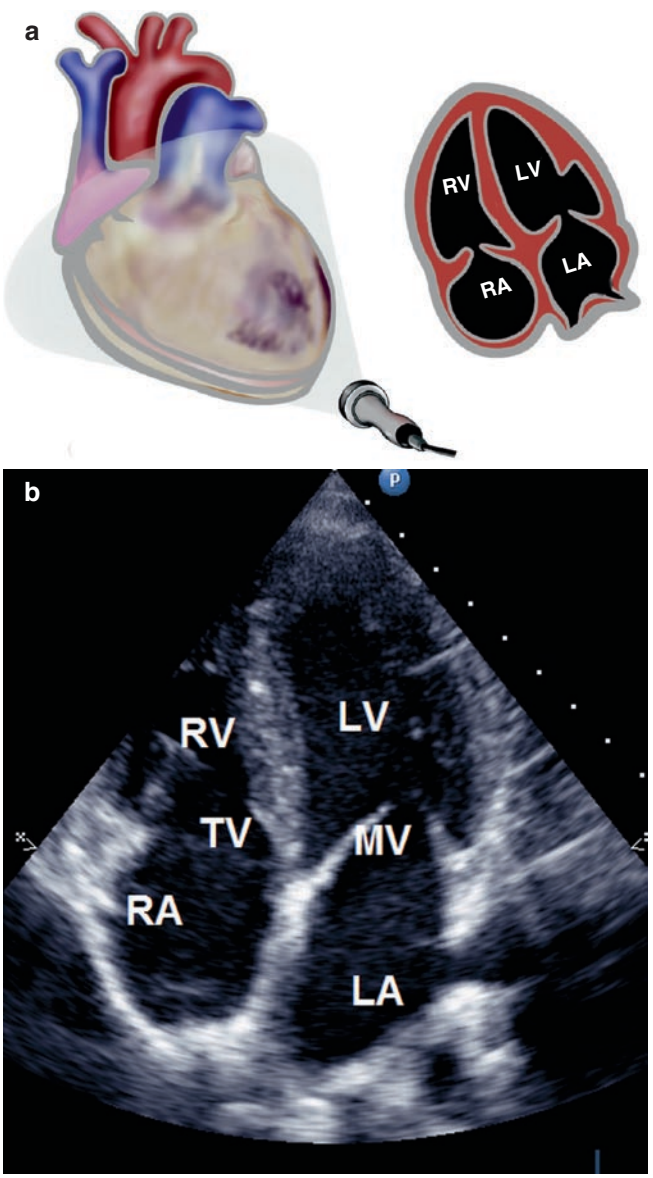

Fig. 1.17 **(a)** Schematic anatomic section of an apical 4-chamber view. **(b)** Corresponding still-frame of a 2D echocardiography apical 4-chamber view. *RV* right ventricle; *LV* left ventricle; *MV* mitral valve; *TV* tricuspid valve

Subsequent clockwise rotation of the transducer about its own axis and with a slight lateral tilt results in 4-, 5-, 2-, and 3-chamber views. Images obtained with the transducer in very high or very medial intercostal spaces should be avoided as they result in truncated ventricular cavity images in which it is not possible to evaluate the ventricular apex.

Apical 4-Chamber View

The apical 4-chamber view (Fig. 1.17) displays all four cardiac chambers, inter-ventricular and inter-atrial septums, mitral and tricuspid valves, and the crux of the heart. The apex and atriums are observed in the image's upper and lower regions, respectively. The right and left cavities of the heart along with their respective atrio-ventricular valves are found in the left and right regions of the image, respectively. In some patients it is possible to observe a transverse cross section of the descending thoracic aorta in the right bottom region of the image.

The mitral valve is usually at a position slightly higher than the tricuspid valve. The anterior mitral leaflet inserts into the left atrio-ventricular groove near the cephalic edge of the membranous septum, while insertion of the septal leaflet of the tricuspid valve occurs 5–10 mm below that of the anterior mitral leaflet. Such anatomical information is useful in identifying ventricular chambers. The entire atrial septum can be observed with a slight anterior re-positioning of the ultrasound beam; this must be done with care because any slight posterior deviation can truncate the image and prevent adequate visualization of the middle segment (region of the *fossa ovalis*). The pulmonary veins can be seen leading to the left atrium in the most posterior region of the image. The image makes possible an optimum analysis of the segmentary contractility of both ventricles through assessments of the lateral wall (in the right region of the image), septum, left ventricular apex, and lateral wall of the right ventricle (Fig. 1.17, Tables 1.3 and 1.4).

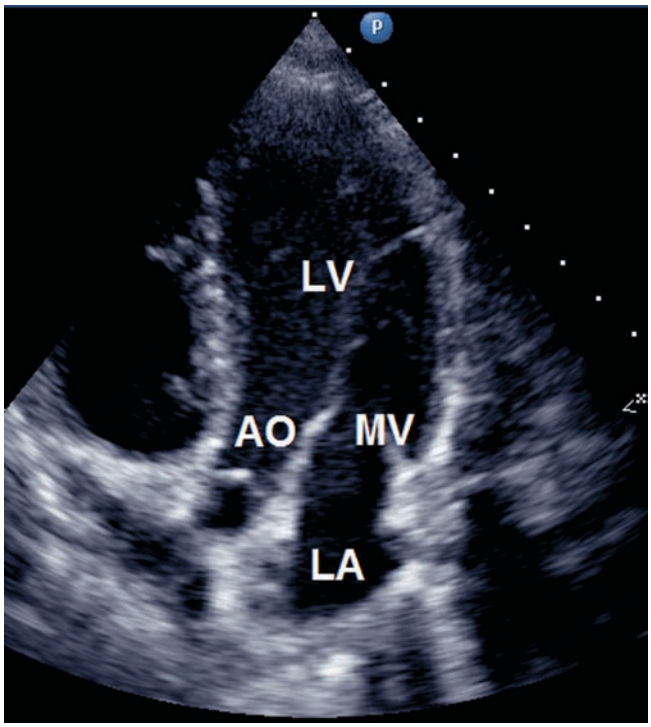

Fig. 1.18 Still-frame of 5-chamber view. We can detect the left ventricular outflow tract, aortic valve, and proximal segment of the ascending thoracic aorta. *MV* mitral valve; *AO* aortic valve; *L* left atrium; *LV* left ventricle

Apical 5-Chamber View

A slight counterclockwise tilt of the transducer makes possible an image of the left ventricular outflow tract, aortic valve, and proximal segment of the ascending thoracic aorta. This section corresponds to the 5-chamber view (Fig. 1.18). The aorta now lies in the position previously occupied by the crux cordis.

Apical 2- and 3-Chamber Views

A 90º counterclockwise rotation of the transducer results in an apical 2-chamber view (Fig. 1.19), in which it is now possible to make an assessment of the left atrium, mitral valve, and left ventricle (anterior and inferior walls in the right and left regions of the image, respectively). Both the apical 2- and 4- chamber views are fundamental in being able to assess segmentary wall motion and left ventricular ejection fraction using Simpson's method. Finally, an apical 3-chamber view can be obtained, in which the aortic valve and aortic root appear in the right portion of the image. This view is similar to the right anterior oblique angiographic projection and has also been called *right anterior oblique equivalent.*

Sub-costal Views

The sub-costal views make possible an assessment of the right and left sides of the heart, which is impossible to obtain

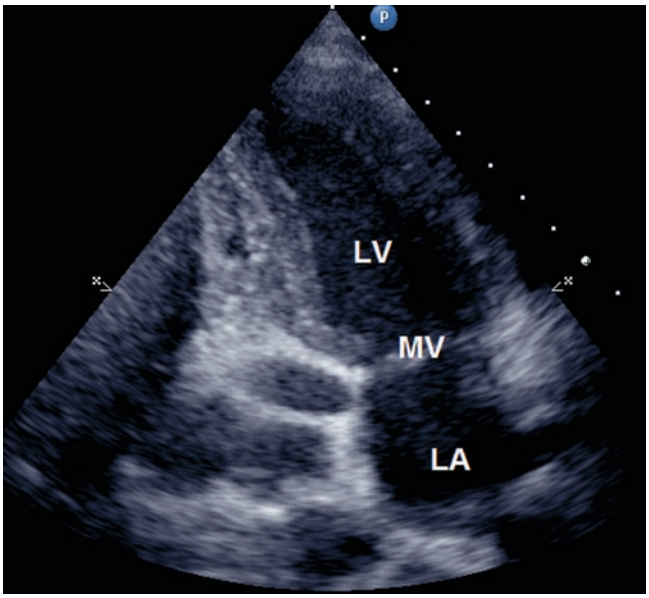

Fig. 1.19 Apical 2-chamber view. *LA* left atrium; *LV* left ventricle; *MV* mitral valve

with parasternal planes. To facilitate the sub-costal imagings, the patient is moved into supine position. Such images are particularly important in patients with chronic obstructive lung disease and emphysema. Figure 1.20 shows the different views obtained from this position: the *sub-costal 4-chamber view* (Fig. 1.20a) is achieved by placing the transducer at the centre of the epigastrium and tilting downward along an imaginary line drawn from the supra-sternal notch to the patient's left shoulder. The image is similar to that of the apical 4-chamber. The plane is especially useful for evaluating defects at the level of atrial septum. The liver is found in the upper region of the image, while below is the right ventricle with its apex directed towards the right. Contractility of the inferior and lateral walls and apex of the right ventricle, as well as the presence of pericardial effusion, can be analyzed.

The tricuspid valve and right atrium can be found to the left of the right ventricle. Wall motion can now be assessed at the septum and left ventricular inferoposterior level. A slight tilting of the transducer results in a 5-chamber view, which makes it possible to observe the left ventricular outflow tract and aortic valve. In the sub-costal view, it is also possible to obtain a section of the abdominal aorta.

An image showing the liver, suprahepatic veins, and transverse cross section of the inferior vena cava can be obtained if the transducer is pointed towards the patient's right side. In order to obtain a long-axis view, it is necessary to point the transducer to the patient's right flank (Fig. 1.20b). In some patients, a very prominent Eustachian valve can be seen in the junction of the inferior vena cava and right atrium.

The short-axis sub-costal view is similar to that of the parasternal. However, it is usually more favourable in the analysis of the right heart (Figs. 1.20c, d).

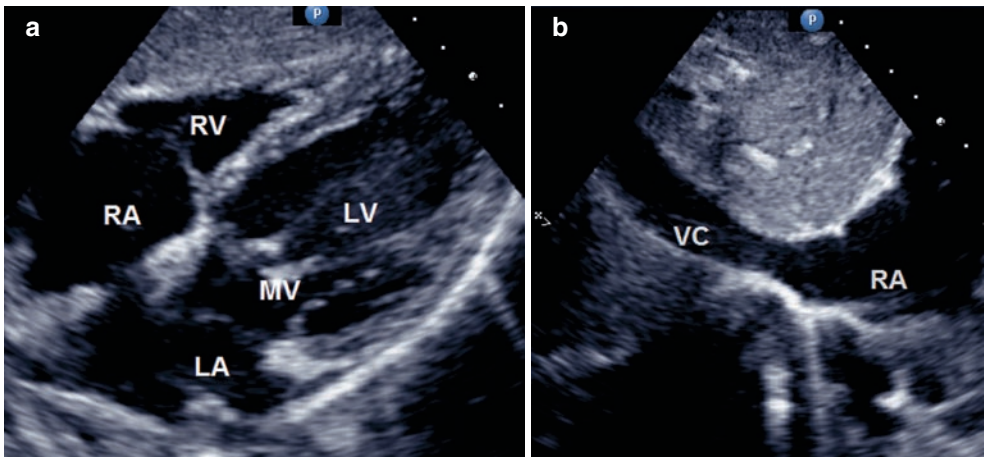

Fig. 1.20 2D echocardiographic images of the different sub-costal views. **(a)** Long-axis view allows a better definition of the atrial septum. **(b)** Entrance to the inferior vena cava to the right atrium. **(c)** Short axis at the basal level in which we can analyze simultaneously the right atrium and the inflow and outflow areas of the right ventricle and pulmonary valve and pulmonary trunk. **(d)** Sub-costal short-axis plane of the left ventricle. *RA* right atrium; *RV* right ventricle; *LA* left atrium; *TV* tricuspid valve; *PV* pulmonary valve; *LV* left ventricle; *MV* mitral valve

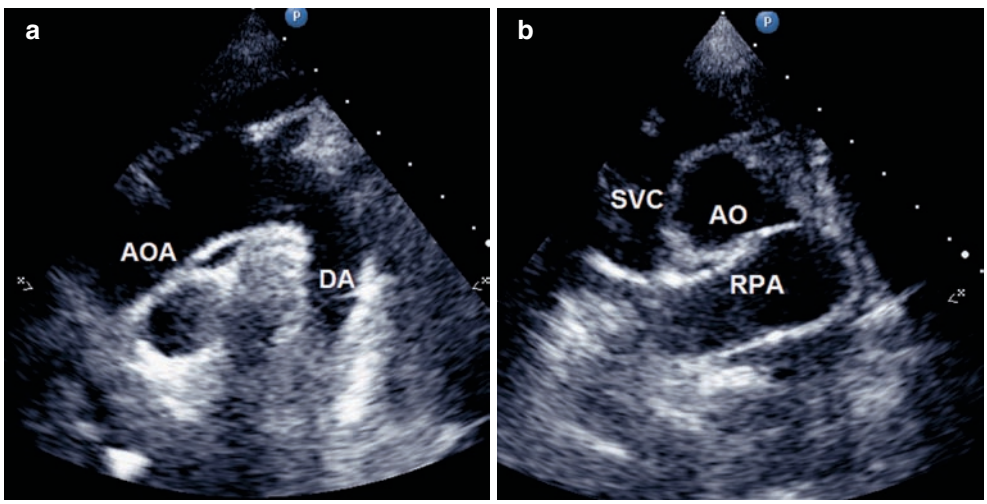

Fig. 1.21 The transducer position in the supraesternal notch allows the visualization of the ascending aorta, aortic arch, brachiocephalic vessel, and descending aorta. **(a)** Long-axis plane through the aorta from the supra-sternal position. **(b)** Short-axis view of the aortic arch. *SVC* superior vena cava; *RPA* right pulmonary artery; *DA* descending thoracic aorta; *AO* aorta

Supra-sternal View

Two different images of the aorta can be obtained if the transducer is placed over the supra-sternal notch (Fig. 1.21). Orientation of the transducer's long axis parallel to the trachea results in the supra-sternal long-axis view. The ascending aorta and aortic arch (with the brachiocephalic vessels) can be seen in the left region of the image, and descending thoracic aorta is found in the right region. The right pulmonary artery and left atrium are seen beneath the aortic arch. A 90º counterclockwise rotation of the transducer allows us a study of the aortic arc. The transverse cross section of the aortic arch is located in the upper region of the image with visualization of the right pulmonary artery in its long-axis format and located inferiorly. A section of the left atrium at the level of its posterior wall as well as the outflow orifice of the right

pulmonary veins can be observed in the extreme lower region of the image. Clockwise rotation of the transducer permits visualization of the superior vena cava appearing along the right side of the aorta.

Other Imaging Planes

It is sometimes necessary to employ unorthodox echocardiographic windows in order to assess certain physiological structures. A right parasternal window may be useful in some patients to permit an assessment of the aorta and inter-atrial septum.[16] A right apical window with the patient placed in the right lateral decubitus position may be useful in cases of dextrocardia.

Doppler Imaging

General Principles

Sound consists of waves. A wave represents the propagation of energy produced by the motion of some specified entity. Sound requires a particle medium, while light does not. Sound (just as any waveform) is defined by several parameters. Wavelength is defined as the distance between corresponding points on two consecutive waveforms (Fig. 1.22).[17,18] The number of waves within a specified unit of time is called the *frequency* and is measured in hertz (Hz or cycles per second). Frequency is inversely proportional to wavelength, i.e. a wavelength of 1 mm would correspond to a frequency of 2 MHz.

The velocity and attenuation of a sound wave depend on both the nature of the medium through which it is propagated and the inherent characteristics of the wave (amplitude and frequency). Transmission of sound in air requires waves of relatively larger amplitude than transmission in a liquid.

In his work of 1842, On the Coloured Light of the Binary Stars and Some Other Stars of the Heavens, Johann Christian Doppler described the changes that are produced in the reception of sound when objects emitting the sound waves are in motion with respect to the listener (Fig. 1.23). A sound's frequency increases and decreases as its source moves towards and away from the observer, respectively. Doppler's theory was initially poorly received. Buys Ballot, a contemporary of Doppler, published a thesis in which he tried to refute Doppler's concept. However, the experiments that he relied upon to do so only further confirmed Doppler's theory.

Doppler cardiac imaging utilizes the Doppler effect as a basis for measuring blood flow velocity in the heart and great vessels. Sound is transmitted through the human body at an almost constant speed. When an ultrasound beam of known frequency (f_0) is transmitted to the heart, a certain percentage of sound is reflected by red blood cells back to the transducer. The reflected wave (f_r) is then analytically compared to the wave originally transmitted. The Doppler Effect predicts that both frequencies will be identical if the red blood cells reflecting the wave are not in motion. The frequency of reflected waves proportionally increases and decreases when red blood cells are moving towards and away from the ultrasound source, respectively. The difference between transmitted and reflected frequencies, known as Doppler shift (Δf), is positive when

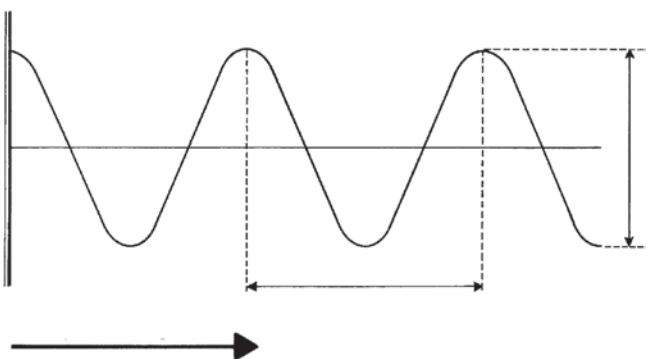

Fig. 1.22 Diagram illustrates the characteristic of sound waves. The frequency and amplitude of particle displacement are expressed as a sine wave

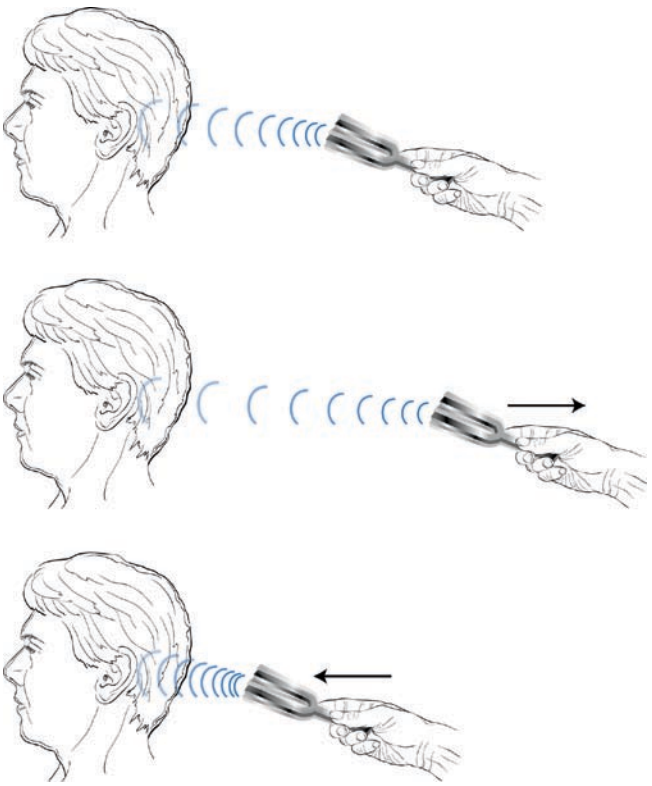

Fig. 1.23 Doppler Effect. A decrease in pitch is perceived as the source moves away from the listener. This is analogous to a reduction in frequency received by the ultrasonic transducer when blood is flowing away from it. An increase in pitch is perceived as the source moves towards the listener. This effect is analogous to an increase in frequency noted when blood moves at a given velocity towards the ultrasonic transducer

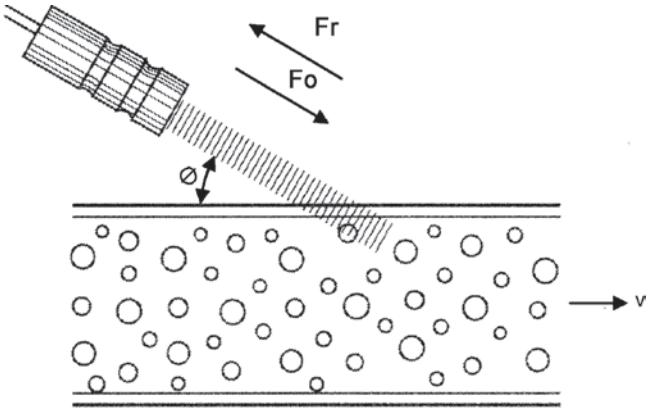

Fig. 1.24 Schematic representation of the Doppler equation

blood flow is towards the transducer and negative when it is away from the transducer. Doppler frequency shift depends on the frequency of ultrasound emission, blood flow velocity, and angle between ultrasound beam and blood flow (Fig. 1.24).

$$\Delta f = 2 f_0 \times v \times \cos\theta / c$$

v = red blood cell velocity, c = speed of sound in blood = 1.560 m/s, f_0 = frequency of transmitted wave, Δf = Doppler shift, θ = angle between ultrasound beam and blood flow. If θ is 0º (i.e. ultrasound beam parallel to blood flow), the cosine value is 1 and maximum blood flow velocity is recorded. Maximum blood flow velocity is progressively under-estimated as θ increases due to corresponding cosine values becoming progressively less than 1. This necessarily results in the under-estimation of Doppler shift, and consequently of peak velocity flow.

Pulsed-Wave Doppler

The two most common forms of Doppler imaging applied to cardiac study are PWD and CWD. In PWD, a single ultrasound crystal emits a short pulse of ultrasound and awaits its return. The pulse is emitted at a specific frequency known as the pulse repetition frequency (PRF) (Fig. 1.25). Although the emission is actually omni-directional in nature, the transducer produces a beam directed and focussed within a determined tri-dimensional area. PWD is accomplished electronically by range gating, which entails transmission of a tone burst at a certain PRF, with selection (gating) for in-line analysis of only those frequencies returning from a discrete portion *(sample volume)* of a cardiac chamber. Blood flow velocity may be determined in different regions by altering the position and size of the sample volume. Relatively larger sample volumes make it easier to detect regions of blood flow, but measurements are relatively non-specific. On the other hand, smaller sample volumes permit more precise spatial analysis of blood

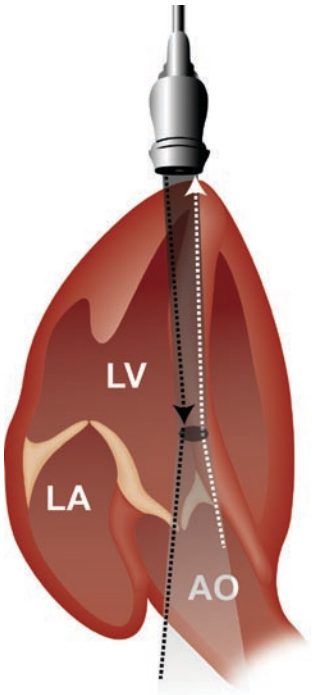

Fig. 1.25 With the pulsed-wave Doppler (PWD), a single ultrasound crystal emits a short pulse of ultrasound and awaits its return before the following pulse is transmitted

flow. The great advantage of PWD is its ability to analyze blood flow at any specific point in the heart cavities, while its chief disadvantage is the limited range of velocities that it can measure. The maximum frequency shift (velocity) that can be exactly measured using a certain PRF is determined by the Nyquist frequency limit, which corresponds to PRF/2. If frequency shift is higher than the Nyquist frequency, *aliasing* is said to occur (Fig. 1.26). The Doppler spectrum gets cut off at the Nyquist frequency limit, and the remaining portion of the signal is recorded on the opposite side of the baseline.

Continuous-Wave Doppler

CWD imaging utilizes a transducer containing two ultrasound crystals–one that continually emits ultrasound pulses and another that continually receives backscattered waveform (Fig. 1.27). Maximum recordable Doppler shift is, in this way, not limited by PRF. The recording can be done with the guidance of 2D echocardiogram or using a small non-imaging transducer (pencil probe). Unlike PWD, CWD measures all frequency shifts present along its beam path. The principal goal of CWD is the complete definition of maximal velocity. However, this advantage is conferred with one important trade-off. Because the wave forms are received and transmitted continuously, no time is allowed for the instrument to discriminate between reception and transmission of a

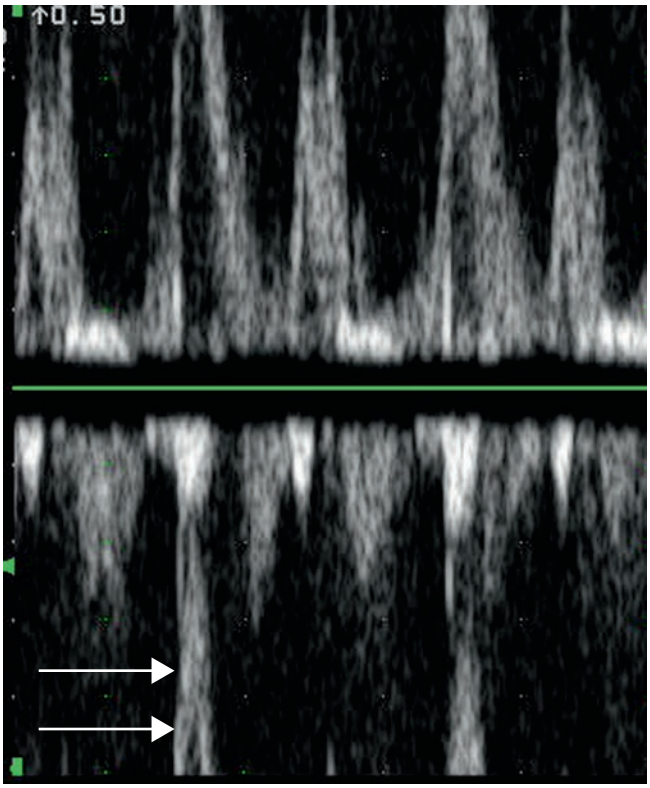

Fig. 1.26 Aliasing effect. Maximal velocity flow of the mitral valve is depicted above 0 baseline, but because of the presence of aliasing, the complexes appear blunted at the top and remaining frequencies are subtracted and plotted at the bottom of the tracing (*arrows*)

given portion of the signal. That means that the use of CWD does not allow localization of specific flow velocity information. Rather, it provides a composite of blood flow velocity information from all sites along the ultrasonic beam.

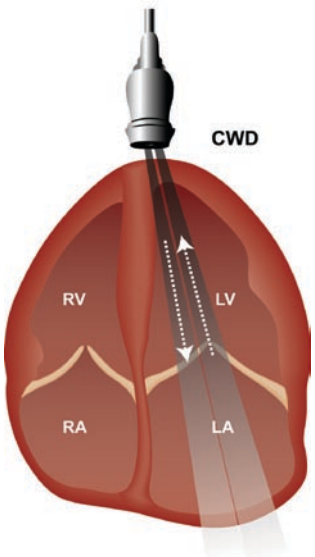

Fig. 1.27 Continuous-wave Doppler imaging utilizes a transducer containing two ultrasound crystals–one that continually emits ultrasound pulses and another that continually receives backscattered waveform

Most blood flow velocities in the normal heart are less than 1.5 m/s and can be measured with precision using PWD. In certain pathological conditions such as valvular stenosis, however, high velocity blood flow jets are common. In this case, it is mandatory to use CWD.

Colour-Flow Doppler

Both pulsed-Doppler and CWD are techniques in which ultrasound pulses are transmitted in a single line. In colour-flow Doppler, however, the ultrasound beam moves through an arc with Doppler shifts being recorded across the entire sector. At every point within the sector, frequency shifts between waves emitted by the transducer and those reflected by red blood cells are assigned certain colour. Colour-flow maps (based on combinations of red, blue, and green) utilizing bidimensional or M-mode images are then constructed in which blood flow velocities are colour coded in function of blood flow turbulence and direction (Fig. 1.28).[19, 20] Blood flow towards the transducer (positive Doppler shift) is represented in red, while blood flow away from the transducer is observed in blue. Maximum blood flow velocities measurable within the Nyquist limit are assigned maximum colour-intensity values. Velocities exceeding the limit produce aliasing and abrupt opposite colourations are observed. Abnormal flows marked by velocity changes and varying degrees of turbulence are represented as mixtures of colours.

Colour-flow Doppler is an important element in the study of cardiac haemodynamics. It not only permits the semi-quantitative estimation of degrees of valvular regurgitation and intra-cardiac shunt, but is also essential in calculations such as that of isovelocity surface area in the quantification of valvular regurgitation. Colour Doppler M-mode is useful in offering a display of abnormal blood flow locations over time.

Normal Colour-Flow Doppler Patterns

Two-dimensional imaging complemented by M-mode is initially assessed. Colour-coded flow imaging is then used for the analysis of intra-cardiac flow.[19–22]

Left Parasternal Long-Axis View

In this imaging plane, the ultrasound beam passes almost perpendicularly through the ventricular wall and aortic and mitral valves. As such, there is little possibility of obtaining good alignment with left ventricular inflow and outflow. The Doppler signal obtained is weak, and data acquired using this imaging plane are limited because colour-flow imaging systems are relatively insensitive to low-velocity blood flows and are consequently more dependent on insonation angles.

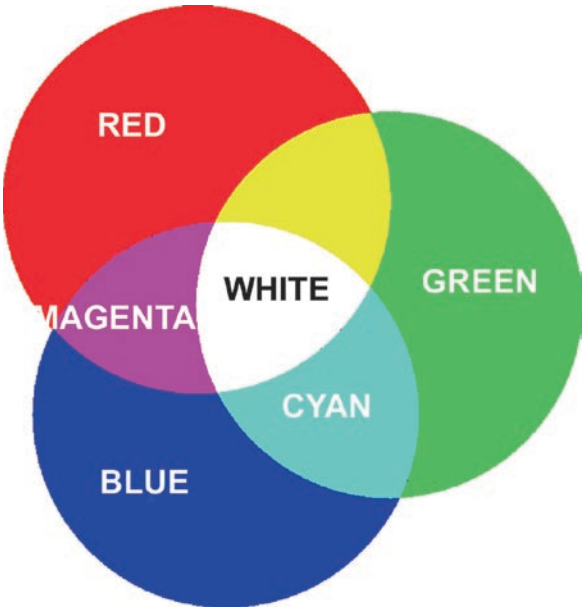

Fig. 1.28 Colour-flow maps (based on combinations of *red, blue,* and *green*) are then constructed in which blood flow velocities are colour-coded in function of blood flow turbulence and direction. Blood flow towards the transducer (positive Doppler shift) is represented in *red*, while blood flow away from the transducer is observed in *blue*

Ventricular and atrial flow is recorded in red during diastole (Fig. 1.29). In the initial phase of ventricular filling, blood flow velocity may be sufficient to cause aliasing and correspond to peak E-wave velocity in M-mode recording of the mitral valve. Retrograde blood flow directed towards the left atrium can be found during mid-diastole and contributes to valve closure. Aliasing disappears during this phase, but reappears following atrial contraction (A-wave). Analysis of this phenomenon over time is more precise upon M-mode rather than 2D images. During systole, a blue-coded column of blood flow can be observed from the left ventricle directed towards the aortic valve within which small aliasing regions can sometimes be detected.

Left Parasternal Short-axis View at Baseline

Left parasternal short-axis view at baseline is one of the most appropriate views for the blood flow analysis of the right cardiac cavities (Fig. 1.30). Blood flow in the right atrium appears in the image as a red-coded column directed towards the tricuspid valve. In the case of tricuspid insufficiency, a blue-coded column of systolic blood flow is observed and directed away from the valve. Right ventricular inflow during diastole is coded in red upon opening of the tricuspid valve and is better analyzed (as in the case of mitral blood flow) using colour M-mode. Blood flow in the right ventricular outflow tract is coded in blue and fills the main pulmonary artery (Fig. 1.31). During diastolic time, it is possible, in normal patients, to observe a small red-coded flow moving towards the right ventricle, which corresponds to a pulmonary insufficiency.

Apical Views

The *apical* views are fundamental (as are those of 2D echocardiography) to the Doppler analysis of intra-cardiac blood flow. A good ultrasound beam alignment with the valvular planes is essential for optimal analysis of Doppler blood flow data at levels of mitral and tricuspid valves, left ventricular outflow tract, and aortic valve.

Blood flow corresponding to atrial filling is observed in red throughout the entire cycle (Fig. 1.32). The blood flow column passes through the atrio-ventricular valvular planes at the onset of diastole and fills the ventricular cavities. Aliasing has been observed at this point in 63% of healthy patients. Colour M-mode inflow analysis permits an evaluation of the relationship between protodiastolic filling (E-wave) and late filling due to atrial contraction (A-wave). In the left ventricle, the blood flow column is directed first towards the lateral ventricular wall and afterwards towards the apex, inter-ventricular septum, and outflow tract. A small region of turbulent flow in contact with the atrial side of the mitral valve can be

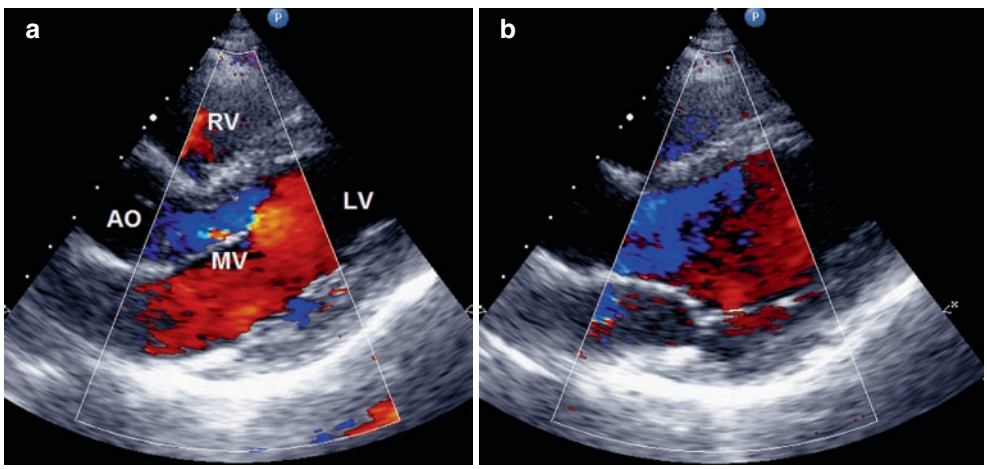

Fig. 1.29 2D echocardiography of the parestenal long-axis view with colour-flow Doppler during **(a)** diastolic frame and **(b)** systolic frame. *Red* flow indicates movement towards the transducer (diastolic filling), and *blue* flow indicates movement away from the transducer (systolic ejection). *AO* aortic valve; *RV* right ventricle; *LA* left atrium; *MV* mitral valve; *LV* left ventricle

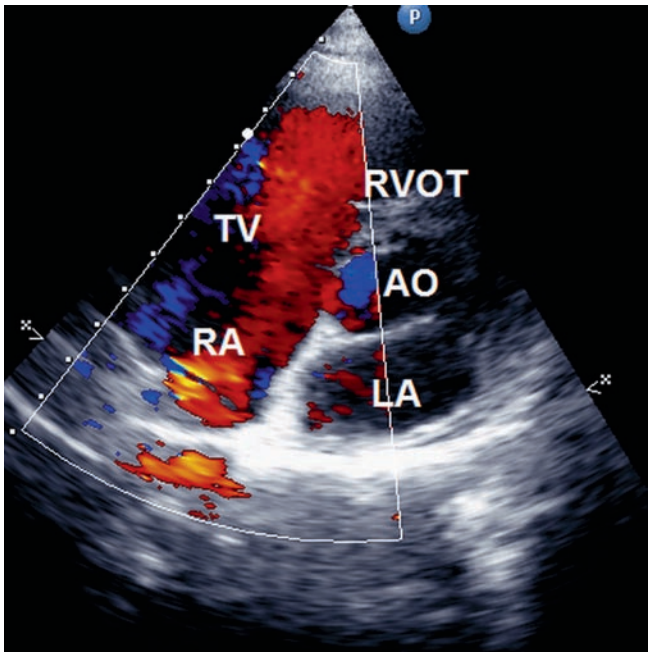

Fig. 1.30 Short-axis view of the aortic valve. The flow can be seen to emerge from the vena cava to the tricuspid valve into the right ventricle. *AO* aortic valve; *RV* right ventricle; *LA* left atrium; *MV* mitral valve; *RVOT* right ventricular outflow tract

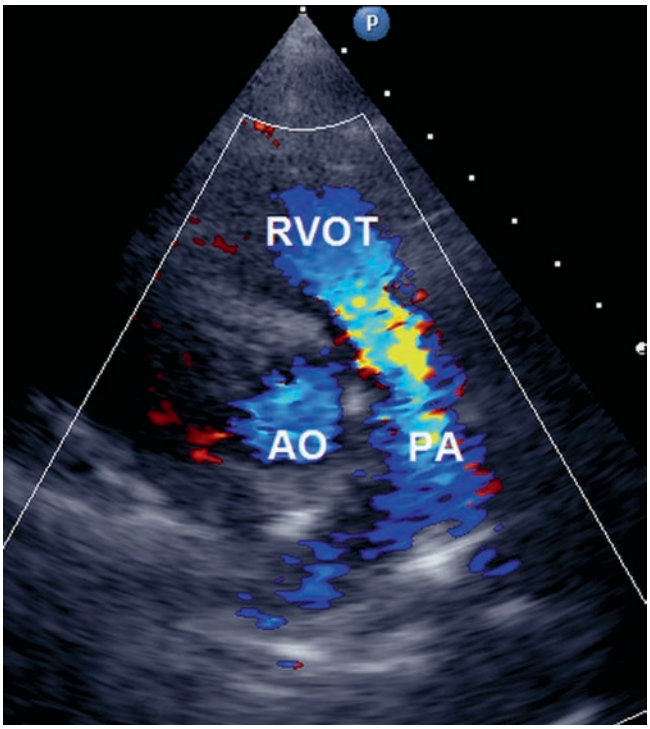

Fig. 1.31 Short-axis view of the aortic valve showing pulmonary outflow tract flow in systole as it fills the pulmonary artery to the bifurcation. *AO* aortic valve; *PA* pulmonary artery; *RVOT* right ventricular outflow tract

observed at the onset of the isovolumetric period.[12] When blood flow moves towards the outflow tract, the direction of motion is away from the transducer, and the column becomes blue-coded. The flow also shows a small region of aliasing near the aortic valve, especially in early systole.

Normal Patterns in Conventional Doppler

Once colour-flow Doppler study has been performed, pulsed-Doppler or occasionally continuous-flow Doppler must be used to study the characteristics of blood flow across the atrio-ventricular valves, great vessels, and heart chambers.

Mitral Valve Flow

Diastolic flow velocity through the mitral valve corresponds with mitral valve morphology as recorded in M-mode echocardiography (Fig. 1.33). There is an initial peak mitral inflow corresponding to passive rapid filling (E-wave) followed by another smaller telediastolic wave due to atrial

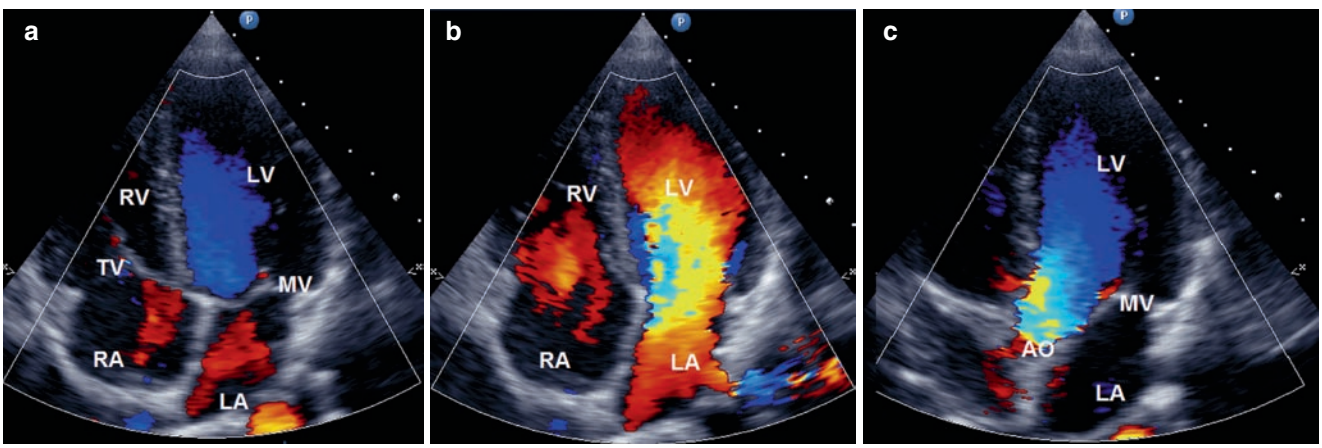

Fig. 1.32 2D echocardiography of the parestenal long-axis view with colour-flow Doppler during **(a)** protodiastole, **(b)** mesodiastole, and **(c)** systole. *Red* flow indicates movement towards the transducer (diastolic filling), and *blue* flow indicates movement away from the transducer (systolic ejection). *AO* aortic valve; *RV* right ventricle; *LA* left atrium; *MV* mitral valve; *LV* left ventricle; *TV* tricuspid valve